

# Spontaneous chiral symmetry breaking in the massive Landau gauge: realistic running coupling

Marcela Peláez,<sup>1</sup> Urko Reinosa,<sup>2</sup> Julien Serreau,<sup>3</sup> Matthieu Tissier,<sup>4</sup> and Nicolás Wschebor<sup>1</sup>

<sup>1</sup>*Instituto de Física, Facultad de Ingeniería, Universidad de la República,  
J. H. y Reissig 565, 11000 Montevideo, Uruguay.*

<sup>2</sup>*Centre de Physique Théorique (CPHT), CNRS,  
Ecole Polytechnique, Institut Polytechnique de Paris,  
Route de Saclay, F-91128 Palaiseau, France.*

<sup>3</sup>*Université de Paris, CNRS, Astroparticule et Cosmologie, F-75013 Paris, France.*

<sup>4</sup>*Laboratoire de Physique Théorique de la Matière Condensée,  
UPMC, CNRS UMR 7600, Sorbonne Universités,  
4 Place Jussieu, 75252 Paris Cedex 05, France.*

(Dated: October 27, 2020)

We investigate the spontaneous breaking of chiral symmetry in QCD by means of a recently proposed approximation scheme in the Landau-gauge Curci-Ferrari model, which combines an expansion in the Yang-Mills coupling and in the inverse number of colors, without expanding in the quark-gluon coupling. The expansion allows for a consistent treatment of ultraviolet tails via renormalization group techniques. At leading order, it leads to the resummation of rainbow diagrams for the quark propagator, with, however, a trivial running of both the gluon mass and the quark-gluon coupling. In a previous work, by using a simple model for a more realistic running of these parameters, we could reproduce the known phenomenology of chiral symmetry breaking, including a satisfactory description of the lattice data for the quark mass function. Here, we get rid of this model-dependence by taking our approximation scheme to next-to-leading order. This allows us to consistently include the realistic running of the parameters and to access the unquenched gluon and ghost propagators to first nontrivial order, which we can compare to available lattice data for an even more stringent test of our approach. In particular, our results for the various two-point functions compare well with lattice data while the parameters of the model are strongly constrained.

PACS numbers: 12.38.-t, 12.38.Aw, 12.38.Bx, 11.10.Kk.

Keywords: Quantum chromodynamics, infrared correlation functions, spontaneous chiral symmetry breaking

## I. INTRODUCTION

Spontaneous chiral symmetry breaking (S<sub>χ</sub>SB) is one of the most prominent aspects of QCD dynamics. It is an emergent infrared phenomenon whose description from first principles goes beyond any (known) perturbative treatment. Our current understanding relies on either lattice simulations [1, 2] or nonperturbative continuum approaches such as truncated Dyson-Schwinger equations (DSE) [3–40], nonperturbative renormalization group (NPRG) techniques [41–46], and the Hamiltonian formalism [47, 48]. Although the latter have reached an impressive level of sophistication and lead to rather successful hadron phenomenology, they often rely on *ad-hoc* approximations that have to be validated *a posteriori*. For instance, the most basic level of description in the context of SDE, based on the so-called rainbow equation for the quark propagator, requires a proper modelling of both the gluon propagator and the quark-gluon vertex [49]. In this context, it is of great interest to identify a systematic organising principle.

In a recent work [50], we have proposed an approximation scheme based on two essential aspects of the infrared QCD dynamics unravelled by lattice simulations and continuum approaches. The first—well-known—observation

is that an expansion in inverse powers of the number of colors ( $N_c$ ) often gives an accurate description of the QCD dynamics. The second point is that the pure gauge running coupling constant, as defined from the Landau gauge ghost-gluon vertex in the Taylor scheme, remains finite and moderate down to deep infrared momentum scales, enabling the use of perturbation theory (see, for instance, Ref. [51]). The concomitant observation that the gluon propagator remains finite at vanishing momentum suggests a simple massive modification of the Faddeev-Popov Lagrangian in the Landau gauge—the so-called Curci-Ferrari (CF) model [52]—as an efficient starting point for a modified perturbative expansion [53, 54].<sup>1</sup> In the last decade, this view has been sup-

---

<sup>1</sup> A modification of the gauge-fixed Lagrangian in the Landau gauge is also expected due to the infamous Gribov ambiguity which makes the Faddeev-Popov Lagrangian an incomplete gauge-fixed description of Yang-Mills theory/QCD at low energies [55]. The various tests that the Curci-Ferrari model has passed suggest that it could be intimately related to the solution of the Gribov puzzle [56]. The connection between Gribov copies and the dynamical generation of a mass term for the gluon field has recently been investigated both in the Landau gauge [57] and

ported by numerous calculations in the perturbative CF model in the vacuum [53, 54, 59–61] and at nonzero temperature [62–65]. Propagators, vertex functions, phase diagrams, etc. have been computed at leading and next-to-leading order and successfully compared to the results of lattice simulations and nonperturbative continuum approaches. Interestingly, these results extend to QCD in the limit of heavy quarks again both at zero and nonzero temperature and the rich phase structure in this regime is again accessible by perturbative methods [66–70]. We also mention that interesting results within the CF approach in Minkowski space have been obtained in Ref. [71]. Also worth mentioning is the related—although quite different in spirit—approach of Refs. [72–74], based on the screened perturbative expansion. Finally, models based on a phenomenological massive gluon exchange have been employed recently in order to analyze the equation of state of neutron stars [75, 76].

In contrast, the light-quark sector is substantially different because the quark-gluon coupling becomes too large in the infrared to allow for a perturbative treatment [77]. To accommodate this feature within a sensible approximation scheme, we have proposed to replace the usual loop expansion in the CF model with a double expansion in the pure gauge coupling and in  $1/N_c$ , keeping the quark-gluon coupling arbitrary [50]. Such a systematic approximation scheme allows for a consistent implementation of renormalization group (RG) techniques, which are crucial to control the ultraviolet (UV) tails of propagators and vertices.

At leading order, the proposed expansion scheme leads to the resummation of the infinite class of rainbow-ladder diagrams in the quark sector, with definite (tree-level) expressions for the gluon propagator and the quark-gluon vertex. However, the running of the associated gluon mass and quark-gluon coupling are trivial (*i.e.*, no running) at this order. In Ref. [50], in order to test the method despite this limitation, we combined the leading order equation for the quark propagator with a simple model for the running gluon mass and quark-gluon coupling. In this paper, we free ourselves from this layer of *ad-hoc* modelling by taking our approximation scheme to next-to-leading order.

While the only effect of the next-to-leading order corrections at the level of the quark propagator is to incorporate a realistic running of the parameters, we now gain access to the gluon and ghost propagators to first nontrivial order. We can then compare our results to available lattice data with no other input parameters than those of the original Lagrangian. The agreement is very good for specific values of these parameters.<sup>2</sup> In particular, this constrains the gluon mass parameter to be nonvanishing

as long as the Yang-Mills coupling remains compatible with simulations.

The article is organized as follows. The CF model and our expansion scheme are briefly reviewed in Sec. II. The next-to-leading order propagators are presented in Sec. III, together with the corresponding anomalous dimensions and running masses, while Sec. IV details the calculation of the beta functions for the couplings in a specific scheme adapted to the propagators. Sec. V presents our results for the running of the parameters and the comparison with the lattice data. We conclude in Sec. VI and a number of technical details are gathered in the Appendices.

## II. MASSIVE LANDAU-GAUGE QCD AND THE RAINBOW-IMPROVED LOOP EXPANSION

As mentioned in the Introduction, lattice simulations of Landau gauge Yang-Mills correlation functions feature a number of interesting properties which have motivated a phenomenological extension of the Faddeev-Popov Lagrangian with the inclusion of a gluon mass term [53, 54]. The corresponding Lagrangian is a particular case of the so-called Curci-Ferrari Lagrangians [52]. The addition of a gluon mass regularizes the infrared and allows for the definition of renormalization schemes without a Landau pole. This property has been used by some of us to compute the two- and three-point correlations functions of the model at one-loop order for all values of momenta [53, 54, 59] and more recently the two-point functions at two-loop order [60], as well as the ghost-antighost-gluon vertex in a particular configuration of momenta [61]. The comparison with lattice data for the Yang-Mills correlation functions turns out to be surprisingly good already at one-loop order, and two-loop corrections further improve the agreement with the data for the two-point functions.

### A. Massive Landau-gauge QCD

In view of these good results within Yang-Mills theory, it is natural to extend these considerations to QCD. Supplementing the usual Euclidean QCD action in the Landau gauge with a gluon mass term yields

$$S = \int d^d x \left[ \frac{1}{4} F_{\mu\nu}^a F_{\mu\nu}^a + i h^a \partial_\mu A_\mu^a + \partial_\mu \bar{c}^a (D_\mu c)^a + \frac{1}{2} m_\Lambda^2 (A_\mu^a)^2 + \sum_{i=1}^{N_f} \bar{\psi}_i (\not{D} + M_\Lambda) \psi_i \right], \quad (1)$$

where  $F_{\mu\nu}^a = \partial_\mu A_\nu^a - \partial_\nu A_\mu^a + g_\Lambda f^{abc} A_\mu^a A_\nu^b$  is the non-abelian field-strength tensor. The covariant derivatives acting on fields in the adjoint ( $X$ ) and fundamental ( $\psi$ )

in a one-parameter family of gauges continuously connected to the Landau gauge [58].

<sup>2</sup> With the noticeable exception of the vector component of the quark propagator; see below.

representations read respectively

$$(D_\mu X)^a = \partial_\mu X^a + g_\Lambda f^{abc} A_\mu^b X^c, \quad (2)$$

$$D_\mu \psi = \partial_\mu \psi - i g_\Lambda A_\mu^a t^a \psi, \quad (3)$$

with  $f^{abc}$  the structure constants of the gauge group and  $t^a$  the generators of the algebra in the fundamental representation, normalized such that  $\text{tr}(t^a t^b) = \delta^{ab}/2$ . We have introduced the notation  $\not{D} = \gamma_\mu D_\mu$ , with Euclidean Dirac matrices  $\gamma_\mu$  such that  $\{\gamma_\mu, \gamma_\nu\} = 2\delta_{\mu\nu}$ . Finally, the parameters  $g_\Lambda$ ,  $M_\Lambda$  and  $m_\Lambda$  are respectively the bare coupling constant, quark mass and gluon mass. For simplicity, we only consider degenerate quark masses. Releasing this assumption is straightforward. For later use, we note  $C_F = (N_c^2 - 1)/(2N_c)$  and  $T_f = 1/2$ .

The previous action is standard, except for the gluon mass term. In actual perturbative calculations, the mass appears only through a modified bare gluon propagator, which reads  $G_{0,\mu\nu}^{ab}(p) = \delta^{ab} G_0(p)(\delta_{\mu\nu} - p_\mu p_\nu/p^2)$ , with

$$G_0(p) = \frac{1}{p^2 + m_\Lambda^2}. \quad (4)$$

The bare ghost propagator is

$$G_{\text{gh},0}^{ab}(p) = \frac{\delta^{ab}}{p^2}, \quad (5)$$

while the bare quark propagator  $S_0(p)$  reads

$$S_0(p) = [-i\gamma + M_\Lambda]^{-1}. \quad (6)$$

Finally, the (unrenormalized) dressed quark propagator can be written as

$$S_\Lambda(p) = [-iA_\Lambda(p)\gamma + B_\Lambda(p)]^{-1} = i\tilde{A}_\Lambda(p)\gamma + \tilde{B}_\Lambda(p), \quad (7)$$

where

$$\tilde{A}_\Lambda(p) = \frac{A_\Lambda(p)}{A_\Lambda^2(p)p^2 + B_\Lambda^2(p)}, \quad (8)$$

$$\tilde{B}_\Lambda(p) = \frac{B_\Lambda(p)}{A_\Lambda^2(p)p^2 + B_\Lambda^2(p)}. \quad (9)$$

The bare propagator (6) corresponds to  $A_\Lambda = 1$  and  $B_\Lambda = M_\Lambda$ .

Despite the excellent results obtained with the model (1) in the quenched limit  $M_\Lambda \rightarrow \infty$ , the corresponding one-loop results in the light-quark sector agree with the lattice data only qualitatively [66, 67]. In fact, the perturbative CF prediction becomes even qualitatively incorrect when the chiral limit is approached: as expected, the perturbative analysis does not reproduce spontaneous chiral symmetry breaking. One possible explanation is that the renormalized coupling constant extracted from the quark-gluon vertex is two to three times larger in the infrared than the one extracted from the ghost-gluon vertex [77], even though, of course, they are both related to the same bare value. It follows that, while the expansion parameter in the Yang-Mills sector was estimated to be about 0.2-0.25 the corresponding one in the quark-gluon sector is of order one [54, 66].

## B. Rainbow-improved loop expansion

In order to take into account these features of the light quark sector we have proposed in Ref. [50] to treat the coupling constants associated to the quark-gluon vertex and to the Yang-Mills vertices on a different footing in the infrared. On the one hand, since perturbation theory reproduces with good accuracy the results of lattice simulations in the Yang-Mills sector, the Yang-Mills coupling constant ( $g_g$ ) can be treated as a small parameter. On the other hand, we refrain from expanding in the quark-gluon coupling ( $g_q$ ) since the latter cannot be considered small.

An obvious problem with this expansion is that it goes beyond any possible analytical treatment. At leading order for instance, it includes already all QED-like diagrams. To overcome this difficulty, we exploited another control parameter present in QCD: we combined our expansion in the pure gauge coupling with an expansion in the inverse number of colors ( $1/N_c$ ). In the large  $N_c$ -limit, the counting is performed after an appropriate rescaling of the couplings,  $g_g = \lambda_g/\sqrt{N_c}$  and  $g_q = \lambda_q/\sqrt{N_c}$ , where  $\lambda_g$  and  $\lambda_q$  are fixed. The added feature of our approach, as compared to the usual  $1/N_c$  expansion, is that  $\lambda_g$  can be treated as another small parameter.

Our asymmetrical treatment of the couplings should not interfere with fundamental properties of QCD in the UV, such as asymptotic freedom or the universality of the running of the coupling. In order to preserve these UV features, we need to make sure that, at a given order of approximation, the expansion contains standard perturbation theory up to a given loop order. In practice, we proceed as follows: we write first all diagrams of standard perturbation theory with up to  $\ell$  loops. Then we count the powers of the Yang-Mills coupling  $\lambda_g$  and of  $1/N_c$  that appear in each of those diagrams and add all diagrams (with possibly more loops) with the same powers of  $\lambda_g$  and  $1/N_c$ .<sup>3</sup> This defines our approximation at  $\ell$ -loop accuracy.

As shown in Ref. [50], the zero-loop order of our approximation scheme leads to tree-level contributions for the gluon and ghost propagators as well as the various vertices, while it resums the rainbow diagrams for the quark propagator, see Fig. 1. That the rainbow equation emerges as the leading order of a systematic expansion is a remarkable result. In particular, this means that corrections to this equation are controlled by two small parameters  $\lambda_g$  and  $1/N_c$ . Also, the rainbow-resummed quark propagator will enter as a basic building block of higher-order contributions. For this reason, we refer to our approximation scheme as the rainbow-improved (RI)

<sup>3</sup> To be precise, what is meant here is the dominant contribution in the naive counting of powers, which excludes possible accidental suppressions; see the example of the quark-gluon vertex below.

FIG. 1: Rainbow equation for the quark propagator obtained both at zero-loop and at one-loop accuracy of our expansion. The thick line represents the dressed quark propagator.

loop expansion.

### C. Renormalization Group and UV tails

The control over higher-order corrections also allows for a consistent implementation of the RG flow. The latter is mandatory in order to obtain a sensible description of UV tails, not suffering from the problem of large logarithms. This is crucial in order to be able to properly remove the UV regulator and avoid the problems pointed out in Ref. [78, 79].

More precisely, let us recall that the RG equation relates the expressions for a given renormalized  $n$ -point vertex function at different renormalization scales. In its integrated form and for the particular case of the propagator associated to a field  $\varphi$ , it reads

$$G_\varphi(p, \mu_0, X_i(\mu_0)) = z_\varphi(\mu, \mu_0) G_\varphi(p, \mu, X_i(\mu)), \quad (10)$$

where  $X_i(\mu)$  denotes the various running couplings and masses of the theory. The benefit of the previous formula is that, in order to evaluate  $G_\varphi(p, \mu_0, X_i(\mu_0))$  in the UV regime ( $p \gg \mu_0$ ) while avoiding large logarithms  $\ln p/\mu_0 \gg 1$ , one can express it in terms of  $G_\varphi(p, \mu, X_i(\mu))$  with  $\mu = p$ , for which large logarithms are absent.

The implementation of the above program requires of course the knowledge of the running of the various parameters together with the scaling factor  $z_\varphi(\mu, \mu_0)$ . The former is controlled by the corresponding beta functions

$$\beta_{X_i} \equiv \mu \frac{d}{d\mu} X_i, \quad (11)$$

where the  $\mu$ -derivative is to be understood at fixed bare values of the parameters  $X_{i,\Lambda} = Z_{X_i} X_i$ . On the other hand, the scaling factor writes

$$z_\varphi(\mu, \mu_0) = \exp \int_{\mu_0}^{\mu} \frac{d\mu'}{\mu'} \gamma_\varphi(\mu'), \quad (12)$$

with

$$\gamma_\varphi \equiv \mu \frac{d}{d\mu} \ln Z_\varphi, \quad (13)$$

the corresponding anomalous dimension, itself defined in terms of the renormalization factor  $Z_\varphi$  that relates the unrenormalized and renormalized versions of the dressed propagator:  $G_{\varphi,\Lambda} = Z_\varphi G_\varphi$ . Both the renormalization

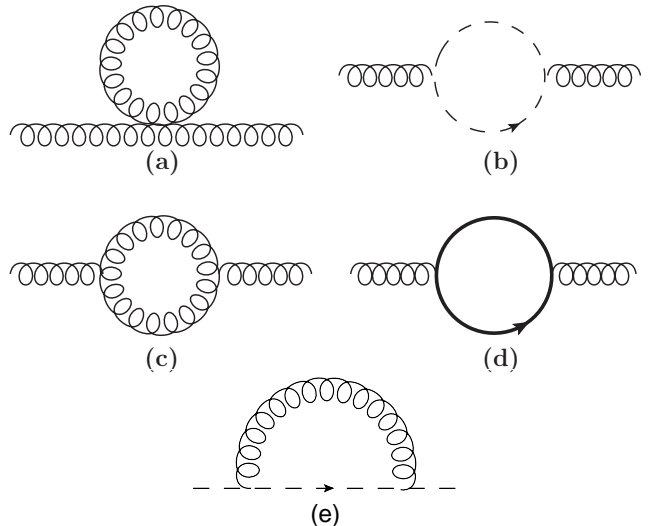


FIG. 2: Diagrams contributing to the gluon (first two lines) and ghost (last line) self-energy at one-loop order of the RI loop expansion. Thick quark lines represent the quark propagator in the rainbow approximation. Diagrams appearing in standard perturbation theory at one loop order look the same but with the quark propagators undressed.

factors and the running parameters depend on the considered renormalization scheme.

In Ref. [50], we have implemented the above program at zero-loop order of the RI-improved expansion. At this order, the running of the gluon mass and of the gauge coupling remain trivial. In this article, we aim at consistently implementing the RG flow of these parameters at lowest nontrivial order. This requires going to next-to-leading (one-loop) order in the RI loop expansion, which we now describe. Since our focus is here on the propagators, we discuss them first in Sec. III, together with the corresponding anomalous dimensions and running masses, before considering the running couplings at the same order in Sec. IV.

## III. PROPAGATORS, ANOMALOUS DIMENSIONS AND RUNNING MASSES

### A. The quark propagator

Interestingly, the one-loop RI approximation for the quark propagator leads exactly to the same equation as the zero-loop order approximation, namely the rainbow equation depicted in Fig. 1. The reason is simply that the tree-level contribution to the quark propagator is of the same order in  $\lambda_g$  and  $1/N_c$  than the one-loop contri-

bution. We then have, writing  $\int_q = \int d^d q / (2\pi)^d$  [50]

$$A_\Lambda(p) = 1 - g_\Lambda^2 C_F \int_{|q| < \Lambda} \tilde{A}_\Lambda(q) \frac{f(q, p)}{(p+q)^2 + m_\Lambda^2}, \quad (14)$$

$$B_\Lambda(p) = M_\Lambda + g_\Lambda^2 C_F \int_{|q| < \Lambda} \tilde{B}_\Lambda(q) \frac{(d-1)}{(p+q)^2 + m_\Lambda^2}, \quad (15)$$

with

$$f(q, p) = \frac{2p^2 q^2 + (d-1)(p^2 + q^2)(p \cdot q) + 2(d-2)(p \cdot q)^2}{p^2 (q+p)^2}. \quad (16)$$

We choose the renormalization factor  $Z_\psi(\mu)$  and the running mass  $M(\mu)$  such that the renormalized dressed propagator obeys

$$S^{-1}(p = \mu, \mu) = -i\cancel{p} + M(\mu), \quad (17)$$

or, in terms of the renormalized components,

$$A(p = \mu, \mu) = 1 \quad \text{and} \quad B(p = \mu, \mu) = M(\mu). \quad (18)$$

We note that  $B(p, \mu)/A(p, \mu) = B_\Lambda(p)/A_\Lambda(p)$  is a scheme-independent quantity. In terms of the renormalized mass introduced above, we have  $B(p, \mu)/A(p, \mu) = B(p, p)/A(p, p) = M(p)$ . It follows that  $M(p)$  has a double interpretation as the renormalized mass in the scheme considered here, or as a scheme-independent quark-mass function.

According to the renormalization group equation (10), the renormalized propagator writes

$$S(p, \mu_0) = z_\psi(p, \mu_0) [-i\cancel{p} + M(p)]^{-1}. \quad (19)$$

The scaling factor can be shown to rewrite as  $z_\psi(p, \mu_0) = Z_\psi(p)/Z_\psi(\mu_0)$ , with

$$Z_\psi(p) = 1 + \frac{g_q^2(p) C_F}{32\pi^2 p^4 m^2(p) Z_\psi(p)} \int_0^\infty dq^2 \frac{Z_\psi(q)}{q^2 + M^2(q)} \left\{ |p^2 - q^2|^3 - m^4(p) [2m^2(p) + 3(p^2 + q^2)] \right. \\ \left. + \sqrt{2q^2 (m^2(p) - p^2) + (m^2(p) + p^2)^2 + q^4} \left[ 2m^4(p) + m^2(p) (p^2 + q^2) - (p^2 - q^2)^2 \right] \right\}, \quad (20)$$

while the running of the quark mass is controlled by

$$\beta_M(p) = \gamma_\psi(p) M(p) - \frac{3g_q^2(p) C_F}{16\pi^2 p^2 Z_\psi(p)} \int_0^\infty dq^2 \frac{Z_\psi(q) M(q)}{q^2 + M^2(q)} \left[ m^2(p) + q^2 - \frac{m^4(p) + m^2(p) (p^2 + 2q^2) - p^2 q^2 + q^4}{\sqrt{m^4(p) + 2m^2(p) (p^2 + q^2) + (p^2 - q^2)^2}} \right]. \quad (21)$$

We refer to Ref. [50] for details. It is important to observe that Eqs. (20) and (21) are UV finite and thus insensitive to the detail of the UV regulator. We show our numerical results for  $Z_\psi(p)$  and  $M(p)$  in Sec. V.

## B. The ghost and gluon propagators

We proceed similarly for the ghost and the gluon propagators at the same order of accuracy. Starting from the standard perturbative one-loop diagrams, depicted in Fig. 2, we include all diagrams with the same powers of  $\lambda_g$  and  $N_c$ . Diagrams (a), (b), (c), and (e), are of order  $\lambda_g^2$  while (d) is of order  $1/N_c$ . It is then easily checked that, in order to improve from standard perturbation theory to the one-loop RI approximation, one only needs to dress the tree-level quark propagators into rainbow-resummed propagators, as indicated by the thick lines used in the

diagram (d).

This means that the ghost propagator remains perturbative at this order, while the gluon propagator involves a perturbative quenched contribution corresponding to diagrams (a), (b), and (c), in addition to the quark loop contribution which we decompose as

$$\Pi_{(d),\Lambda}^{\rho\sigma}(p) = \left( \delta_{\rho\sigma} - \frac{p_\rho p_\sigma}{p^2} \right) \Pi_{(d),\Lambda}^\perp(p) + \frac{p_\rho p_\sigma}{p^2} \Pi_{(d),\Lambda}^\parallel(p). \quad (22)$$

The appearance of a longitudinal contribution coming from the quark sector is a novel feature with respect to the strict one-loop calculation. In the former case, one can exploit an exact Slavnov-Taylor identity between the bare longitudinal inverse gluon propagator and the bare ghost dressing function [54]

$$\Gamma_{\parallel,\Lambda}^{(2)}(p) F_\Lambda^{-1}(p) = m_\Lambda^2, \quad (23)$$

to argue that the quarks do not contribute to the longitudinal gluon propagator at one-loop order (since there are no corrections from the quarks to the ghost dressing function at this order). This identity is broken at one-loop order of the RI expansion, thus leading to a spurious longitudinal contribution from the quark sector (despite the fact that the ghost dressing function remains the same as before). Because the transverse gluon propagator coincides with the longitudinal one in the zero-momentum limit, this spurious contribution affects the transverse propagator as well. In order to cope with this issue, we proceed as follows. We first note that the divergences of  $\Pi_{(d),\Lambda}^{\rho\sigma}$  are those of the corresponding one-loop contribution, see App. B. In particular,  $\Pi_{(d),\Lambda}^{\parallel}$  is finite and will be denoted  $\Pi_{(d)}^{\parallel}$  in what follows. Second, we devise a renormalization scheme such that the renormalized mass parameter  $m$  is not directly influenced by the spurious longitudinal contributions. To this purpose, we impose the following renormalization conditions on the renormalized dressed ghost and gluon propagators:

$$G_{\text{gh}}^{-1}(p = \mu, \mu) = \mu^2, \quad (24)$$

$$G^{-1}(p = \mu, \mu) = \mu^2 + m^2(\mu) + \Pi_{(d)}^{\parallel}(p = \mu). \quad (25)$$

We have checked that not including the longitudinal quark contribution in the RHS of (25) leads to a singular behavior of the gluon propagator at zero momentum.

When evaluating the renormalized gluon propagator, there is, in principle, a factor  $Z_A(\mu)$  that multiplies  $\Pi_{(d)}^{\parallel}(p = \mu)$ . The latter can be set to 1 at the present order of approximation, that is, up to corrections of order  $\lambda_g$  or  $1/N_c$ . We find that the quark loop contributes a term

$$\delta Z_A^{(d)} = -\frac{\Pi_{(d),\Lambda}^{\perp}(p = \mu) - \Pi_{(d)}^{\parallel}(p = \mu)}{\mu^2} \quad (26)$$

to  $Z_A$ , on top of the renormalization factor in the quenched case. It follows that

$$\gamma_A = \gamma_A^{\text{quench.}} - \mu \frac{d}{d\mu} \left( \frac{\Pi_{(d),\Lambda}^{\perp}(p = \mu) - \Pi_{(d)}^{\parallel}(p = \mu)}{\mu^2} \right), \quad (27)$$

where  $\gamma_A^{\text{quench.}}$  is the quenched anomalous dimension obtained from diagrams (a)-(c), already determined in Ref. [54]. We stress that the  $\mu$ -derivative is to be understood at fixed bare quantities. Since  $\Pi_{(d),\Lambda}^{\perp}(p = \mu)$  and  $\Pi_{(d),\Lambda}^{\parallel}(p = \mu)$  are expressed only in terms of bare quan-

ties, this derivative is easily computed.<sup>4</sup> We obtain

$$\begin{aligned} \gamma_A(\mu) = \gamma_A^{\text{quench.}} &+ 8 \frac{g_q^2(p) T_f N_f}{Z_\psi^2(p)} \frac{d}{dp^2} \left( \frac{1}{p^2} \int_q \frac{Z_\psi(q)}{q^2 + M^2(q)} \right. \\ &\times \left. \frac{Z_\psi(\ell)}{\ell^2 + M^2(\ell)} \left\{ \frac{1}{d-1} \left[ d \frac{(p \cdot q)^2}{p^2} - q^2 \right] + q \cdot p \right\} \right)_{p=\mu}, \end{aligned} \quad (28)$$

where  $\ell = p + q$ . Another important consequence of the finiteness of  $\Pi_{(d)}^{\parallel}$  is that, despite (23) not being fulfilled at one-loop order of the RI expansion, the divergent part of  $Z_A Z_{m^2}$  is equal to that in the strict one-loop expansion. In this later case, Eq. (23) imposes that  $Z_A Z_{m^2} Z_c$  should be finite [54, 80–83], which we can trivially extend to the present case since  $Z_c$  also coincides in the strict one-loop and RI one-loop approximations. We shall then fix the running of the gluon mass through the condition

$$Z_A Z_c Z_{m^2} = 1. \quad (29)$$

This implies

$$\beta_{m^2} = m^2(\gamma_A + \gamma_c). \quad (30)$$

We mention that the nonrenormalization theorem underlying (29) arises as a consequence of a BRST-like symmetry present in the Curci-Ferrari model which require the use of dimensional regularization. Because  $\gamma_c$  is perturbative, it can be computed using dimensional regularization. In contrast, since  $\gamma_A$  contains a nonperturbative contribution, it is not obvious *a priori* how dimensional regularization should be implemented. We discuss this issue in Appendix A.

#### IV. RUNNING COUPLINGS

We now discuss the running of  $g_q$ , needed to close the set of equations (20) and (21), and that of  $g_g$ , which is inevitably coupled to the running of  $m$ .

##### A. The pure-gauge coupling

We fix the coupling constant  $g_g$  in the ghost-gluon sector using the Taylor scheme  $\sqrt{Z_A Z_c} Z_{g_g} = 1$  [84], which implies

$$\beta_{g_g} = g_g \left( \frac{\gamma_A}{2} + \gamma_c \right). \quad (31)$$

Together with (24), (25), and (30), this defines the so-called infrared-safe scheme [54]. In this scheme, the anomalous dimensions can be expressed linearly in terms

<sup>4</sup> To the present order of accuracy, we can set  $Z_\psi Z_g = \sqrt{Z_A Z_c} Z_g = 1 + \mathcal{O}(\lambda_g, 1/N_c)$  when obtaining Eq. (28).

FIG. 3: Some of the diagrams contributing to the quark-gluon vertex at one-loop order of the RI loop expansion (see Appendix B for the complete list). The thick line represents the quarks propagator in the rainbow approximation. Diagrams in standard perturbation theory at one-loop order are the same, however, with quark propagators undressed.

of the beta functions. This in turn implies that  $z_A(p, \mu_0)$  and  $z_c(p, \mu_0)$  have simple expressions in terms of the running parameters, so that

$$G_{\text{gh}}(p, \mu_0) = \frac{m^2(\mu_0)}{g_g^2(\mu_0)} \frac{g_g^2(p)}{m^2(p)} \frac{1}{p^2} \quad (32)$$

and

$$G(p, \mu_0) = \frac{g_g^2(\mu_0)}{m^4(\mu_0)} \frac{m^4(p)}{g_g^2(p)} \frac{1}{p^2 + m^2(p) + \Pi_{(d)}^{\parallel}(p)}, \quad (33)$$

and we need only to focus on the running parameters in this case.

The explicit expression for  $\Pi_{(d)}^{\parallel}$  in the RI-one loop order can be obtained with the same procedure. We get ( $\ell = p + q$ )

$$\begin{aligned} \Pi_{(d)}^{\parallel}(p) = & -8 \frac{g_g^2(p) T_f N_f}{Z_\psi^2(p)} \int_q \frac{Z_\psi(q)}{q^2 + M^2(q)} \frac{Z_\psi(\ell)}{\ell^2 + M^2(\ell)} \\ & \times \left\{ -\frac{(p \cdot q)^2}{p^2} + \frac{q \cdot (q - p)}{2} + \frac{M(q) M(\ell)}{2} \right\}. \end{aligned} \quad (34)$$

## B. The quark-gluon coupling

The beta function for the quark-gluon coupling is obtained from the quark-antiquark-gluon vertex function. The one-loop contributions are represented in Fig. 3 and are of (naive) order  $\lambda_g^2 N_c^{-1/2}$  for diagram (a) and  $N_c^{-3/2}$  for diagram (b). As explained before, to consistently evaluate the vertex function at next-to-leading (one-loop) order in the RI loop expansion, one must supplement these diagrams with all higher loop diagrams with the same parametric dependence in  $\lambda_g$  and  $N_c$ . This involves infinite series of ladder diagrams which we discuss in Appendix B. Although interesting, because some of these resummations include a nontrivial source of flavour dependence, this calculation lies beyond the scope of the present work. The focus here is on the propagators, and as we now explain, a consistent calculation of the running coupling that enters the latter at the present order of approximation does not necessarily require the calculation of these diagrams, provided one chooses an appropriate renormalization scheme.

Our resummed approximation scheme is devised so as to exactly reproduce the standard loop expansion in the

UV, where all couplings are to be treated on the same footing. The essential point here is that the diagram (b) of Fig. 3 is UV finite and, thus, does not contribute to the beta function in the UV. As a consequence, we can always devise a renormalization scheme where the coupling is defined from diagram (a) only, without spoiling the UV structure of the theory at one-loop order. Following our general procedure, in such a scheme, we only have to supplement this diagram—and not diagram (b)—with the higher loop diagrams of the same order in  $\lambda_g$  and  $N_c$ . A detailed inspection shows that this simply amounts to dressing the internal quark lines with rainbow insertions, that is, to replacing the internal quark line by the rainbow-resummed quark propagator, as depicted by the thick line in Fig. 3.

Of course, the corresponding renormalization factor  $Z_{g_q}$  does not allow to render the quark-gluon vertex finite at this order of approximation, but because our focus is here on the two-point functions, this choice remains consistent. Moreover, we mention that the explicit calculation of the color factors reveals that the diagram (b) of Fig. 3 receives a further suppression by one power of  $1/N_c$  as compared to the naive counting and is thus of the same order  $N_c^{-5/2}$  as next-to-next-to-leading order (non-planar) diagrams in our expansion scheme. The coupling defined in the scheme described here is therefore an accurate description of the one that would result from the full vertex.

We denote the corresponding quark-gluon vertex by  $\Gamma_{\bar{\psi}\psi A_\mu^a}(p, r, k)$ , with  $k$  the gluon momentum,  $p$  the quark momentum and  $r$  the anti-quark momentum (all incoming). It can be decomposed into twelve independent tensorial structures. Here, we follow the convention of Ref. [85] and write

$$\Gamma_{\bar{\psi}\psi A_\mu^a}^\Lambda(p, r, k) = t^a \Gamma_\mu^\Lambda(p, r, k), \quad (35)$$

with

$$\Gamma_\mu^\Lambda(p, r, k) = -ig_\Lambda \left( \sum_{i=1}^4 \lambda_i^\Lambda L_{i\mu} + \sum_{i=1}^8 \tau_i^\Lambda T_{i\mu} \right). \quad (36)$$

The various tensorial structures  $L_{i\mu}$  and  $T_{i\mu}$  are given in Table I.

We choose to define the renormalized quark-gluon coupling constant through the scalar function [85]

$$\lambda_1'^\Lambda = \lambda_1^\Lambda - k^2 \tau_3^\Lambda, \quad (37)$$

that is, we choose a transverse vertex (where the gluon is contracted with a transverse projector).<sup>5</sup> We make this choice in order to define the coupling through a vertex that can be extracted directly from Landau-gauge lattice

<sup>5</sup> Moreover, we normalize the coupling in order that it coincides with the bare vertex at tree-level.

Coupling	Tensorial structure
$\lambda_1$	$L_{1\mu} = \gamma_\mu$
$\lambda_2$	$L_{2\mu} = -(\not{p} - \not{r})(p - r)_\mu$
$\lambda_3$	$L_{3\mu} = -i(p - r)_\mu$
$\lambda_4$	$L_{4\mu} = -i\sigma_{\mu\nu}(p - r)_\nu$
$\tau_1$	$T_{1\mu} = i(k_\mu r_\nu k_\nu - r_\mu k^2)$
$\tau_2$	$T_{2\mu} = (k_\mu r_\nu k_\nu - r_\mu k^2)(\not{p} - \not{r})$
$\tau_3$	$T_{3\mu} = \not{k}k_\mu - k^2\gamma_\mu$
$\tau_4$	$T_{4\mu} = -i[k^2\sigma_{\mu\nu}(p - r)_\nu - 2k_\mu\sigma_{\nu\lambda}r_\nu k_\lambda]$
$\tau_5$	$T_{5\mu} = i\sigma_{\mu\nu}k_\nu$
$\tau_6$	$T_{6\mu} = \not{k}(p - r)_\mu - k_\nu(p - r)_\nu\gamma_\mu$
$\tau_7$	$T_{7\mu} = -\frac{i}{2}k_\lambda(p - r)_\lambda[(\not{p} - \not{r})\gamma_\mu - (p - r)_\mu] - i(p - r)_\mu\sigma_{\nu\lambda}r_\nu k_\lambda$
$\tau_8$	$T_{8\mu} = -\gamma_\mu\sigma_{\nu\lambda}r_\nu k_\lambda + r_\mu\not{k} - \not{r}k_\mu$

TABLE I: The different tensorial structures along which the quark-gluon vertex is decomposed, together with the associated (scalar) coupling constants.

simulations. On top of the choice of tensorial structure, one needs to choose a momentum configuration. We consider the case where the quark and antiquark momenta are orthogonal and of equal norm (OTE, orthogonal two-equal configuration). In this momentum configuration, the coupling  $\lambda_1^\Lambda(p)$ , where, again,  $p$  is the quark momentum, can be extracted from lattice simulations as

$$\lambda_1'^\Lambda(p) = \frac{\text{Im} \text{tr}[\gamma_\sigma \Gamma_\mu^\Lambda(p, r, k) P_{\mu\nu}^\perp(k) P_{\nu\rho}^\perp(r) P_{\rho\sigma}^\perp(p)]}{4g_\Lambda(2-d)}, \quad (38)$$

where the right-hand-side is to be evaluated in the OTE configuration. We detail the calculation of  $\lambda_1'^\Lambda(p)$  in Appendix C.

The renormalized quark-gluon coupling is then defined as

$$g_q(\mu) = Z_\psi \sqrt{Z_A} g_\Lambda \lambda_1'^\Lambda(\mu), \quad (39)$$

from which we deduce the beta function

$$\beta_{g_q} = g_q \left( \gamma_\psi + \frac{1}{2}\gamma_A + \frac{d \ln \lambda_1'^\Lambda}{d \ln \mu} \right). \quad (40)$$

The RI expansion at one-loop order is constructed so as to contain the standard one-loop contributions in the UV. In this spirit, it is consistent to replace  $d \ln \lambda_1'^\Lambda / d \ln \mu \simeq d \lambda_1'^\Lambda / d \ln \mu$  at the present level of precision since  $\lambda_1'^\Lambda = 1 + \mathcal{O}(\lambda_g, 1/N_c)$ . Moreover, after taking the  $\mu$ -derivative, we can replace bare masses and couplings by renormalized ones, using similar remarks as above. It is important to stress that the flow of  $g_q(\mu)$  depends on the full momentum-dependence of the quark propagator and vice-versa, so their coupled equations need to be solved simultaneously together with the flow for  $g_g(\mu)$  and  $m(\mu)$ . In Appendix A, we show that  $\beta_{g_g}$ ,  $\beta_{g_q}$ , and  $\beta_m$  have the known one-loop expressions in the UV.

## V. RESULTS

In this section, we solve the rainbow equation numerically, together with the flow of the gluon mass and coupling constants. We proceed by successive iterations from a given ansatz until a required accuracy is reached. The momentum integrals over  $q$  are divided into two regions  $q \leq \mu_0$  and  $\mu_0 < q < \Lambda$ . In the former, we sample the functions  $Z_\psi(p)$  and  $M(p)$  on a regular grid with a lattice spacing  $\delta q$  whereas we use, for the latter, the known UV expressions (solutions of the rainbow equations [50])

$$Z_\psi^{\text{UV}}(q) = 1, \quad (41)$$

$$M^{\text{UV}}(q) = b_0 \left( \ln \frac{q^2 + m_0^2}{m_0^2} \right)^{-\alpha} + \frac{b_2}{q^2} \left( \ln \frac{q^2 + m_0^2}{m_0^2} \right)^{\alpha-1}, \quad (42)$$

where [4, 50]

$$\alpha = \frac{N_c^2 - 1}{2N_c} \frac{9}{11N_c - 2N_f}, \quad (43)$$

and  $b_0$  and  $b_2$  are constants adjusted at each iteration step so that  $M(p)$  is continuous and differentiable at  $\mu_0$ . The term proportional to  $b_0$  dominates the UV behaviour for a nonzero bare quark mass whereas the term  $\propto b_2$  is the dominant one in the chiral limit. We also use the previous expressions as an initial condition for the iteration while keeping  $M(\mu_0)$  fixed.

There are, *a priori*, four free parameters:  $M(\mu_0) = M_0$ ,  $m(\mu_0) = m_0$ ,  $g_g(\mu_0) = g_0$  and  $g_q(\mu_0)$ . In fact, the latter two are not independent since they both relate to the one and only bare coupling constant of the model  $g_\Lambda$ . Taking  $\mu_0$  in the UV regime and using perturbation theory in the present scheme, one obtains (see Appendix D for details)

$$g_q(\mu_0) = g_g(\mu_0) \left( 1 + \frac{N_c g_g^2(\mu_0)}{64\pi^2} [5 - 3 \log 2] \right) \quad (44)$$

where we neglected terms of order  $g_g^5(\mu_0)$  and  $g_g^3(\mu_0) \times m^2/\mu_0^2$ . Note that  $g_q(\mu_0) > g_g(\mu_0)$ .

We now compare our numerical results for the  $SU(3)$  quark and gluon propagators within the one-loop RI scheme with available lattice data for two degenerate light quarks,  $N_f = 2$  [2, 86].

### A. Quark propagator

We first investigate the parameters  $M_0$ ,  $m_0$ ,  $g_0$  which best fit the lattice data for the quark mass function. For this purpose, we fix  $M_0$  as the lattice value at the momentum closest to  $\mu_0 = 10$  GeV. We also choose  $\Lambda = 30$  GeV and  $\delta p = 0.05$  GeV. We have tested that our results are stable against changes of  $\mu_0$ ,  $\Lambda$  and  $\delta p$ .

We then scan for different values of  $m_0$  and  $g_0$  while minimizing the following error function

$$\Delta^2 = \frac{1}{2N_{lt}} \sum_{i=1}^{N_{lt}} \left[ \frac{1}{\bar{M}_{lt}^2} + \frac{1}{M_{lt}^2(i)} \right] [M_{lt}(i) - M(i)]^2, \quad (45)$$

where the sum runs over the  $N_{lt}$  lattice momenta below 1 GeV. Here,  $M_{lt}(i)$  denote the quark mass function measured on the lattice and  $\bar{M}_{lt}$  its value at the lowest lattice momentum, where it reaches its maximum.

As an example, we show in Fig. 4 the error levels using  $M_0 = 3$  MeV and lattice data from Ref. [2] either in terms of the parameters  $m_0$  and  $g_0$  at the scale  $\mu_0$  or in terms of the RG evolved parameters  $m(\mu)$  and  $g(\mu)$  at the scale  $\mu = 1$  GeV. We observe that one can fit the quark mass data with relatively low values of the gluon masses. However, below a certain threshold, our numerics becomes unstable suggesting the presence of an infrared Landau pole (as observed in the Yang-Mills case [87]). What happens is the following: A low gluon mass tends to increase the effective interaction between quarks and to favour the spontaneous breaking of chiral symmetry. However, if the gluon mass becomes too small the RG flow of the coupling is not regular anymore and no solution is found. The parameters that minimize the error function (45) are  $m_0 = 0.08$  GeV and  $g_0 = 1.9$ , or, equivalently,  $m(\mu) = 0.12$  GeV and  $g_g(\mu) = 2.42$ , giving  $\Delta = 0.07$ . The range of parameters giving a similar level of precision, with  $\Delta < 0.1$ , is shown in Fig. 4.

In Fig. 5, we compare the quark mass function  $M(p)$  obtained in the present approach with lattice data from Ref. [2]. The agreement is excellent. To be fair, we mention that the one-loop expression of  $M(p)$  is also able to give a rather good description of the lattice data, as shown in Fig. 6. This, however, requires pushing the parameter  $m_0$  and  $g_0$  to rather large values, incompatible with values from other fits. For instance, the unquenched gluon propagator is badly described with such large gluon mass values.

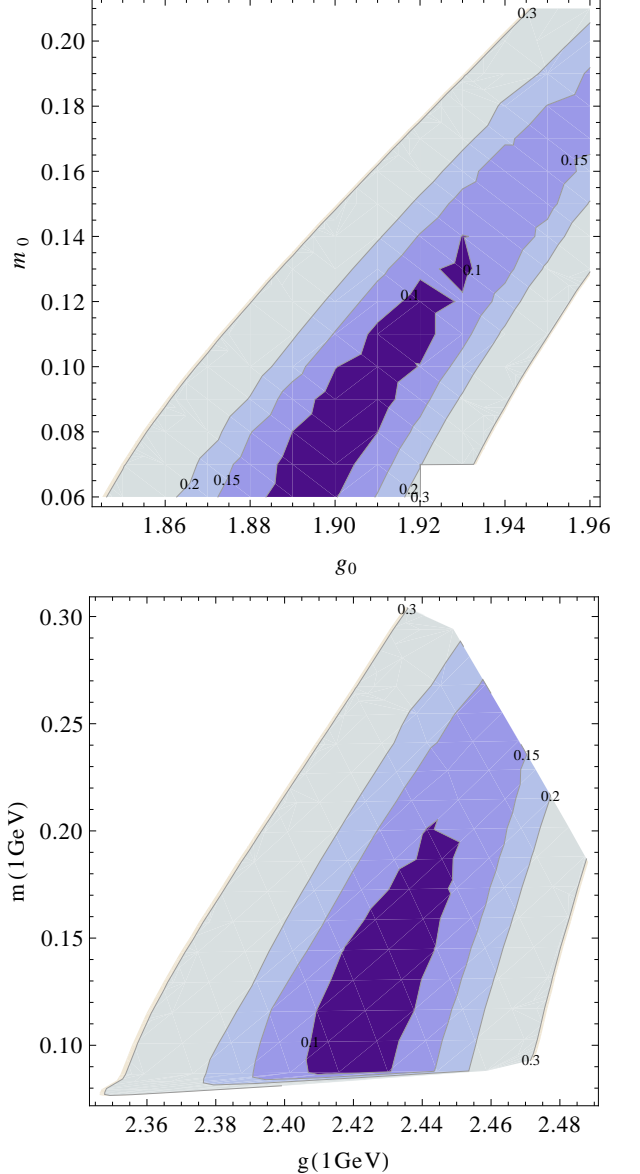


FIG. 4: Top: Contour levels for the error function  $\Delta$  obtained using chiral data from [2] and  $M_0 = 3$  MeV, for different values of  $m_0$  and  $g_0$ . Bottom: The same contours in terms of the running parameters  $m(\mu)$  and  $g(\mu)$  at the scale  $\mu = 1$  GeV. The darkest region corresponds to parameters with  $\Delta < 0.1$ . All masses are given in GeV.

### B. Gluon propagator

We now focus on the gluon propagator. We fit the expression (33) of the gluon dressing function  $p^2 G(p)$  against the lattice data of Ref. [86]. Similarly to Eq. (45) we define an error function associated to the gluon propagator as

$$\Delta_G^2 = \frac{1}{2N_{lt}} \sum_{i=1}^{N_{lt}} \left[ \frac{p^4(i)}{\mu^4 \bar{G}_{lt}^2} + \frac{1}{G_{lt}^2(i)} \right] [G_{lt}(i) - G(i)]^2 \quad (46)$$

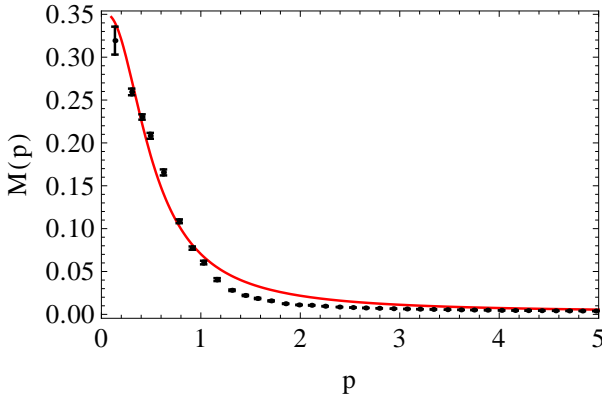


FIG. 5: The function  $M(p)$  compared to the lattice data from Ref. [2]. The best fit parameters are  $M_0 = 3$  MeV,  $m_0 = 0.08$  GeV, and  $g_0 = 1.9$ , corresponding to  $\Delta = 0.07$ .

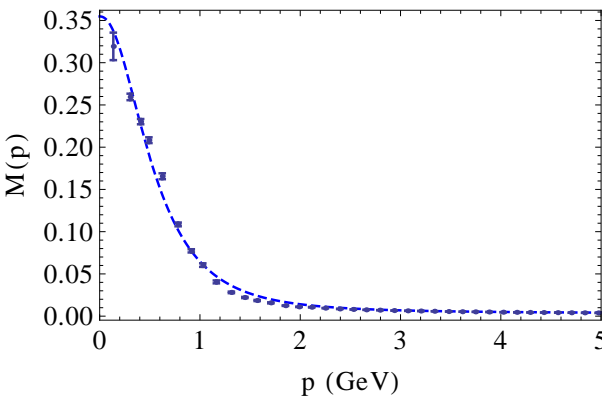


FIG. 6: The RG-improved one-loop expression of Ref. [66] for  $M(p)$  can be employed to describe well lattice data. This necessitates to push the gluon mass to artificially large values, here,  $m_0 = 780$  MeV and  $g_0 = 2.625$ .

where the sum runs over the  $N_{lt}$  lattice momenta below 3 GeV. Here,  $p(i)$  is the lattice momentum corresponding to the point  $i$ ,  $G_{lt}(i)$  denotes the gluon propagator measured on the lattice at the same point and  $\tilde{G}_{lt}$  its value at the lattice momentum  $\mu$  closest to 1 GeV *i.e.*, near the maximum of the dressing function.

At first, we perform fits of the gluon propagator alone, independently of the quark mass function. The corresponding contour plots are shown in Fig. 7. As for the quark mass function, there exist regions of parameters giving excellent fits. The best-fit values (keeping  $M_0 = 3$  MeV as before) are  $m_0 = 0.2$  GeV and  $g_0 = 1.89$  or, equivalently,  $m(\mu) = 0.39$  GeV and  $g(\mu) = 4.67$  at  $\mu = 1$  GeV, which gives  $\Delta_G = 0.03$ . The corresponding gluon propagator is shown in Fig. 8. As for the quark mass function, the gluon dressing function can be fitted with good accuracy with a one-loop calculation [66] (taking into account RG effects). Here, though, the best-fit parameters are sensibly the same than for the RI-one-loop case. However, using the RI one-loop expression for the fit is important in order to assess the internal consis-

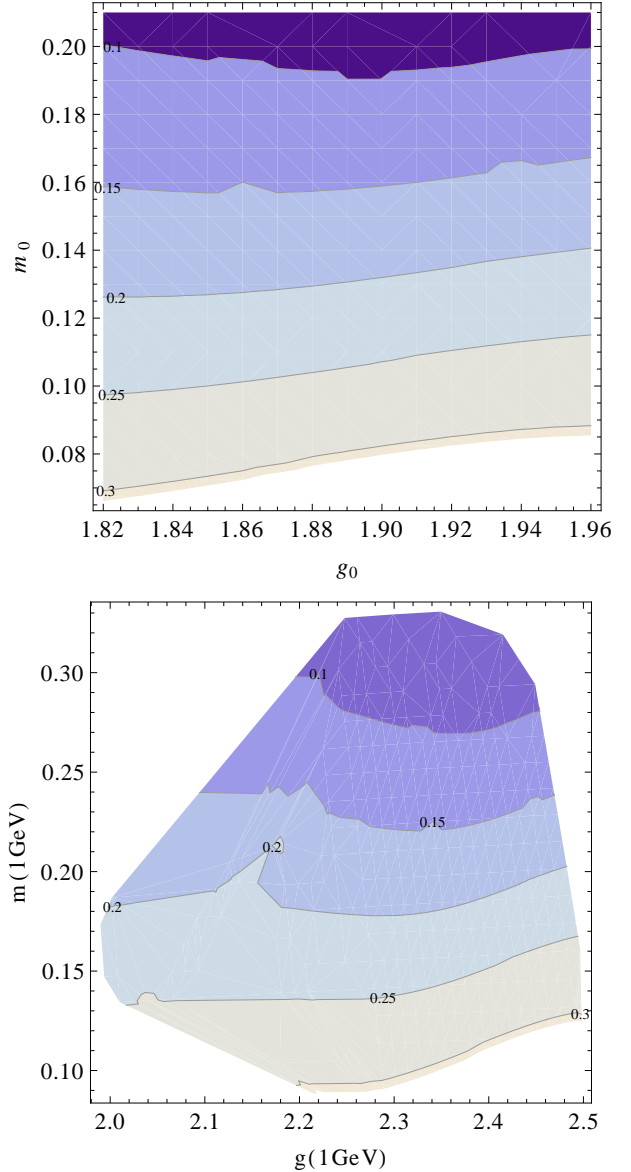


FIG. 7: Top: Contour levels for the error function  $\Delta_G$  obtained using chiral data from [86] and  $M_0 = 3$  MeV, for different values of  $m_0$  and  $g_0$ . Bottom: The same contours in terms of the running parameters  $m(\mu)$  and  $g(\mu)$  at the scale  $\mu = 1$  GeV. The darkest region corresponds to parameters with  $\Delta_G < 0.1$ . All masses are given in GeV.

tency of our approximation scheme.

### C. Quark and gluon propagators combined

The previous results show that one can obtain excellent fits of either the quark mass function or the gluon propagator. However, we point out that the approximations involved in the present order of the RI scheme are not expected to give such small values of the error functions  $\Delta$  and  $\Delta_G$ . In fact, fitting a single correlation function

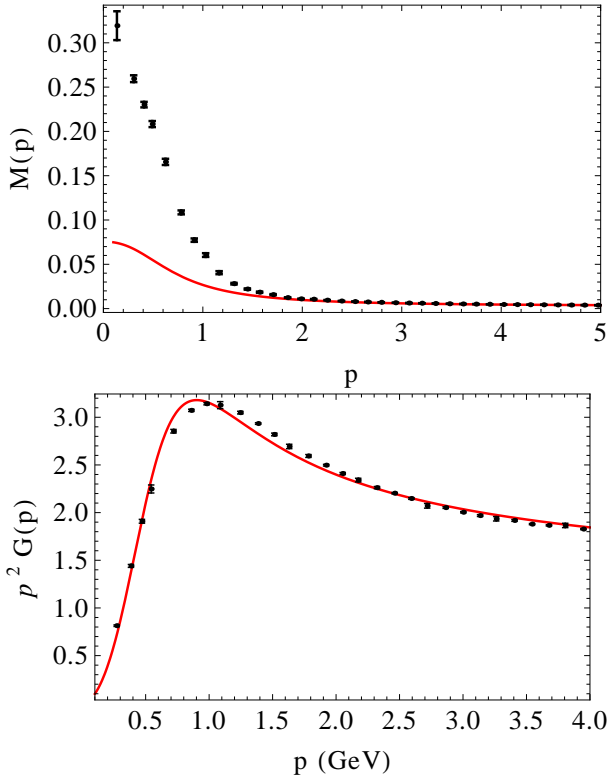


FIG. 8: Quark mass function  $M(p)$  (top) and gluon dressing function  $p^2 G(p)$  (bottom) compared with lattice data from [86]. The best fit parameters are (for  $M_0 = 3$  MeV)  $m_0 = 0.2$  GeV and  $g_0 = 1.89$ , corresponding to  $\Delta_G = 0.03$ .

at a time can give artificially good results. Indeed, we observe in Figs. 4 and 7 that the regions of parameters giving good fits for the two functions separately do not overlap. This is illustrated in Fig. 9. Good fits for the gluon propagator require sensibly higher values of the gluon mass than for the quark mass function. In order to obtain a realistic control of the quality of our approximation, it is desirable to fit all available lattice data with a single set of parameters. When fitting the quark mass function and the gluon propagator together, we find regions of parameters for which both the error estimators  $\Delta$  and  $\Delta_G$  are below 15%. The best parameters for this combined fit are (using  $M_0 = 3$  MeV),  $m_0 = 0.15$  GeV and  $g_0 = 1.94$  or, equivalently,  $m(\mu) = 0.21$  GeV and  $g(\mu) = 2.45$  for  $\mu = 1$  GeV. The corresponding quark mass and gluon dressing functions are shown in Fig. 9. The overall agreement remains quite satisfactory.

An important general observation is that it is not possible to reproduce lattice data with a gluon mass (defined at the scale  $\mu = 1$  GeV) smaller than 200 MeV. In fact, the favorable values are typically of the order of 250 MeV if we insist on fitting simultaneously the quark mass and the gluon propagator.

In Fig. 10, we show the function  $z_\psi(p, \mu_0)$  for the best fit parameters obtained above as compared to the corresponding lattice data. In contrast to the quark mass

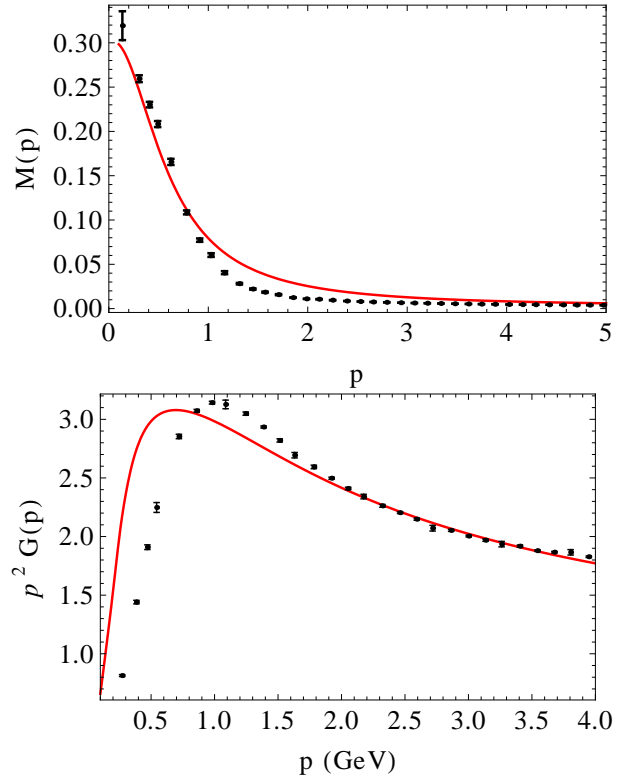


FIG. 9: Quark mass function  $M(p)$  (top) and gluon dressing function  $p^2 G(p)$  (bottom) compared with lattice data from [2] and [86], respectively, using  $M_0 = 3$  MeV,  $m_0 = 0.15$  GeV and  $g_0 = 1.94$ .

function, the latter is not well reproduced. The reason for this mismatch has been discussed at length in Refs. [50, 66] in the context of perturbation theory. The difficulty to obtain the function  $z_\psi$  is common to most analytical approaches and is related to the fact that, in the Landau gauge, this function is dominated by two-loop diagrams that are not included at the present order of approximation.

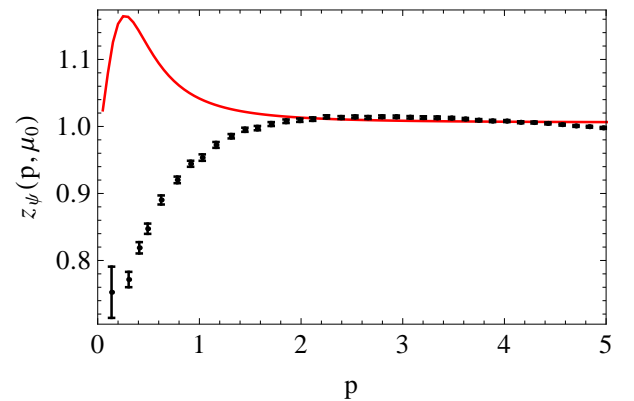


FIG. 10: The function  $z_\psi(p)$  normalized to  $z_\psi = 1$  at  $p = 2$  GeV for the set of parameters  $M_0 = 0.003$  GeV,  $m_0 = 0.15$  GeV and  $g_0 = 1.94$ .

Finally, we show, in Fig. 11, the running of the quark-gluon and ghost-gluon couplings, as well as the gluon mass for the best fit parameters. We see that the quark-gluon coupling is systematically larger than the ghost-gluon one which is consistent with the assumptions underlying our expansion scheme. Moreover, in perturbation theory, the relevant expansion parameter is  $(g^2 N_c)/(16\pi^2)$ . For the ghost-gluon coupling the running never exceeds a comfortable  $(g_g^2 N_c)/(16\pi^2) \lesssim 0.12$  whereas it reaches  $(g_q^2 N_c)/(16\pi^2) \approx 0.68$  for the quark-gluon coupling and a perturbative treatment appears much more questionable.<sup>6</sup>

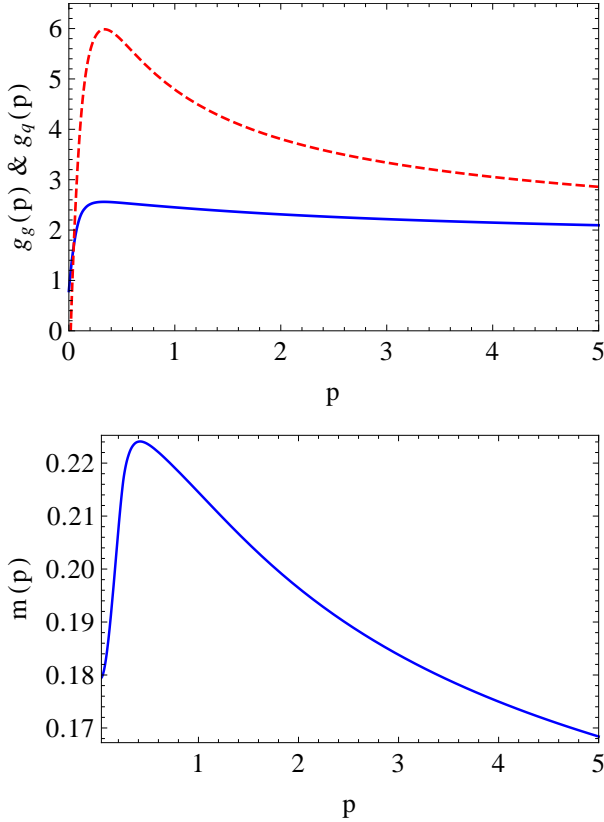


FIG. 11: Top: flow of the coupling constants  $g_g(p)$  (plain) and  $g_q(p)$  (dashed). Bottom: flow of the gluon mass  $m(p)$ . The parameters are  $M_0 = 0.003$  GeV,  $m_0 = 0.15$  GeV and  $g_0 = 1.94$ .

## VI. CONCLUSIONS

In Ref. [50] we proposed a systematic expansion scheme, dubbed the RI loop expansion, in order to study the infrared QCD dynamics within the Curci-Ferrari

model. The RI expansion scheme relies on a double expansion using  $g_g$  and  $1/N_c$  as small parameters that allows for a consistent implementation of the renormalization group. In Ref. [50], we implemented this approach at leading order with, however, the caveat that the running of the various parameters was modelled by hand. In the present article, we go one step beyond by considering the RI expansion at next-to-leading (one-loop) order, treating the running of the parameters in a consistent way leaving, in particular, only the parameters of the Lagrangian  $M_0$ ,  $m_0$ , and  $g_0$  as free adjustable parameters. We compare our results for the quark and gluon propagators with existing lattice data near the chiral limit [2, 86]. We find regions of parameters of the CF model which simultaneously describe the quark mass function and the gluon propagator with good precision.

An important observation is that we obtain a consistent solution where the ghost-gluon coupling remains perturbative due to the gluon propagator that shows a massive behavior. When adjusting the parameters to the lattice data, it is observed that a massless gluon is not compatible with the solution of the rainbow equation for the quark mass function. Indeed, below a certain value of the gluon mass, the equations become numerically unstable suggesting the appearance of an infrared Landau pole. Moreover, even before reaching those instabilities the gluon propagator becomes very badly reproduced. That is, with gluon masses below 200 MeV one cannot reproduce with a reasonable precision the gluon propagator. Instead, favorable values for the gluon mass (at the scale 1 GeV) in order to fit simultaneously the quark mass function and the gluon propagator are of the order of 250 MeV. This is consistent with the value obtained both in the Yang-Mills and in the heavy quark sector.

We also computed the beta function for the quark-gluon coupling in a particular renormalization scheme where we can discard the diagram (b) of Fig. 3 and its diagrammatic completion (see Appendix B). This is sufficient for what concerns the calculation of the propagators. Computing the quark-gluon vertex function would require the evaluation of further diagrams, including the proper treatment of their renormalization. On the technical side the diagram (b) of Fig. 3 is both UV finite and receives an additional suppression in  $1/N_c$  as compared to its naive scaling. Of course, in principle, it is interesting to consider other renormalization schemes which include this diagram and its diagrammatic completion. In that case, it is worth mentioning that only part of the diagrammatic completion is further suppressed by  $1/N_c$  as compared to the naive order. As shown in the Appendix B, there exists an infinite class of ladder diagrams of order  $N_c^{-3/2}$ , part of which actually corresponds to an effective one-meson exchange. Interestingly, such diagrams yield a nontrivial flavor dependence already at the present order of approximation and may be of genuine interest for that reason.

As a future application of this expansion scheme, we plan to evaluate mesonic properties. In particular, at

<sup>6</sup> We note that those values are slightly smaller than those obtained in previous studies in the quenched approximation and in the case of heavy quarks [54, 66].

one-loop order in the RI expansion, the meson-quark-antiquark vertex is described by the rainbow-ladder approximation for the Bethe-Salpeter equation [50]. Moreover, the present approach can be extended to analyze the thermal and finite density properties of quark-gluon matter. First steps in this direction have been made in Ref. [88].

### Acknowledgments

The authors would like to acknowledge the financial support from PEDECIBA and ECOS program and from the ANII-FCE-126412 project. NW and MP would like to acknowledge the support and hospitality of École Polytechnique, where part of this work has been realized. UR and JS acknowledge the support and hospitality of the Universidad de la República de Montevideo during the latest stages of this work. Part of this work also benefited from the support of a CNRS-PICS project “irQCD”.

### Appendix A: Gluon anomalous dimension

We discuss how the gluon anomalous dimension (28) is computed using dimensional regularization. We show that it is finite and that it coincides with the one-loop anomalous dimension in the UV. Since the quenched contribution is perturbative, the only issue is how to treat the contribution from the quark loop.

To this purpose, we write  $M^2(p) = M^2 + \Delta M^2(p)$  and  $Z_\psi(p) = 1 + \Delta Z_\psi(p)$  such that

$$\begin{aligned} \frac{Z_\psi(q)}{q^2 + M^2(q)} &= \frac{1}{q^2 + M^2} & (A1) \\ &+ \frac{\Delta Z_\psi(q)}{q^2 + M^2(q)} - \frac{\Delta M^2(q)}{(q^2 + M^2)(q^2 + M^2(q))}, \end{aligned}$$

where we note that the second line is suppressed by an extra factor of  $q^2$  in the UV as compared to the first line ( $\Delta Z_\psi(q) \sim 1/q^2$  see below). Since the original integral in Eq. (28) is quadratically divergent, this means that the potential divergences involve at most one insertion of this second line. Moreover, in all the terms where the divergence is logarithmic we can take the limit  $p \rightarrow 0$  and replace  $M(q)$  by  $M$  in the denominators. This yields the following potentially divergent terms

$$\begin{aligned} &\int \frac{d^d q}{(2\pi)^d} \frac{1}{q^2 + M^2} \frac{1}{\ell^2 + M^2} \\ &\times \left\{ \frac{2}{d-1} \left[ \frac{(p \cdot q)^2}{p^2} - q^2 \right] + q \cdot \ell + M^2 + \Delta M^2(q) \right\} \\ &+ 2 \int \frac{d^d q}{(2\pi)^d} \left[ \frac{\Delta Z_\psi(q)}{(q^2 + M^2)^2} - \frac{\Delta M^2(q)}{(q^2 + M^2)^3} \right] \\ &\times \left\{ \left( 1 - \frac{2}{d} \right) q^2 + M^2 \right\}, & (A2) \end{aligned}$$

where, again,  $\ell = p + q$  and we have used the symmetry of the integrand upon  $q \leftrightarrow \ell$ . Combining some terms this rewrites as

$$\begin{aligned} &\int \frac{d^d q}{(2\pi)^d} \frac{1}{q^2 + M^2} \frac{1}{\ell^2 + M^2} \\ &\times \left\{ \frac{2}{d-1} \left[ \frac{(p \cdot q)^2}{p^2} - q^2 \right] + q \cdot \ell + M^2 \right\} \\ &+ \left( \frac{4}{d} - 1 \right) \int \frac{d^d q}{(2\pi)^d} \frac{\Delta M^2(q)}{(q^2 + M^2)^2} \\ &+ 2 \left( 1 - \frac{2}{d} \right) \int \frac{d^d q}{(2\pi)^d} \frac{\Delta Z_\psi(q)}{(q^2 + M^2)}, & (A3) \end{aligned}$$

where we have again considered  $p \rightarrow 0$  where appropriate and we have thrown finite parts. The first line is nothing but the standard perturbative one loop expression and can be evaluated using dimensional regularization. Let us now show that the remaining integrals are UV finite.

The integral in the second line is finite for  $d < 4$  but has a logarithmic divergence when  $d \rightarrow 4$ . However, the pre-factor proportional to  $4 - d$  makes the full result finite when the regulator is removed. The same mechanism does not hold for the integral in the third line and its convergence crucially depends on the properties of  $Z_\psi(q)$ . In the Landau gauge, for  $q \gg m$ , the function  $Z_\psi(q)$  behaves, at one loop, as (see, for instance, Ref. [66])

$$Z_\psi(q) = 1 + ag_q^2(q) \frac{m^2(q)}{q^2} + \dots & (A4)$$

where the corrections are of order  $1/q^4$  up to logarithms. It is easily checked from Eq. (20) that this remains true at one-loop order in the RI expansion Owing to the fact that, at large momenta [67],

$$g_q^2(q) \propto 1/\log(q^2), \quad m^2(q) \propto [1/\log(q^2)]^{35/44}, & (A5)$$

the third integral in (A3) is convergent in the limit  $d \rightarrow 4$ . It is important to note, however, that the convergence is slow and there are important relative contributions at very large momenta. This could make the associated result doubtful. However, even if the numerical estimate of this integral can be difficult, the overall contribution of the UV tail is numerically small (this is because the main contribution comes from momenta  $q \lesssim M$ ).<sup>7</sup>

<sup>7</sup> One possible origin for the slow convergence of the integrals could be the miscancellation of UV divergences in the perturbative diagrams that are resummed in the rainbow approximation. Indeed, mis-cancelled perturbative subdivergences can sum up to slowly convergent expressions [89]. For instance, the quark-loop in the gluon propagator contains a two-loop contribution where a one-loop quark self-energy is inserted in one of the lines of the loop. By opening up the gluon line in this self-energy, one generates a contribution to the four-gluon function which is not finite and does not have the structure of the four-gluon tree-level vertex. The reason why this occurs is that there are missing channels

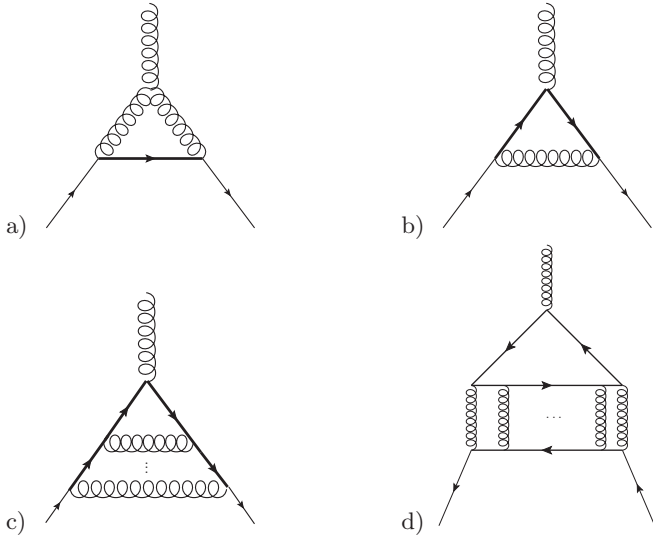


FIG. 12: Diagrams contributing to the quark-gluon vertex at one-loop order of the RI loop expansion. The thick line represents the quarks propagator in the rainbow approximation. Diagrams in standard perturbation theory at one-loop order are obtained from diagrams (a) and (b) after undressing the quark propagators.

Another consequence of the above is that the behavior of the anomalous dimension matches its one-loop expression in the UV. Owing to Taylor's theorem, the same holds true for the beta function  $\beta_{g_s}$ .

## Appendix B: The quark-gluon vertex

Even though this is not the main focus of the present work, for completeness, we discuss here the diagrams that contribute to the quark-gluon vertex at next-to-leading (one-loop) order of the RI expansion. We first determine how the standard one-loop diagrams scale with our expansion parameters  $\lambda_g$  and  $1/N_c$ . Then we proceed to their diagrammatic completion, that is, we identify all higher-loop diagrams with the same scalings.

The two possible one-loop contributions are identical to diagrams (a) and (b) in Fig. 12 but with bare quark propagators instead of dressed ones. The naive power counting in our expansion parameters yields  $\lambda_g^2 N_c^{-1/2}$  for diagram (a) and  $N_c^{-3/2}$  for diagram (b). A careful inspection shows that including higher-loop diagrams with the same respective powers amounts to dressing all internal quark lines with rainbow-resummed propagators, dressing the quark-gluon vertex in diagram (b) with infinitely many one-gluon exchange rungs, as shown in di-

agram (c), and resumming the infinite ladders with the topology of diagram (d). Again, all internal quark lines in diagrams (c) and (d) are rainbow-resummed quark propagators.

The explicit calculation of the color factors reveals a further suppression by one power of  $1/N_c$  for the diagrams (b) and (c), which are actually of the same order  $N_c^{-5/2}$  as higher order nonplanar diagram. Another important property is that these diagrams are UV-finite and do not contribute to the beta function in the UV. In contrast, the diagrams (d) do not receive any additional suppression by  $1/N_c$  and are actually UV divergent. They thus contribute to the beta function for the quark-gluon coupling in the UV, however, starting at two-loop order. As explained in the main text, it is thus consistent to devise a scheme for the running quark-gluon coupling at one-loop order in the RI expansion without these diagrams. However, they should be included in a calculation of the full quark-gluon vertex at the present order of approximation. It is interesting to note that these diagrams, contrarily to the previous ones (a), (b), and (c), yield a nontrivial flavor dependence since they are proportional to the number of flavors  $N_f$ . We also note that the infinite series of ladder diagrams presents meson poles and the diagrams (d), thus, include an effective one-meson exchange contribution. It is interesting that such contributions, directly sensitive to the flavor structure of the theory, appear already at this order of approximation in our expansion scheme.

## Appendix C: Calculation of $\lambda_1'^\Lambda(p)$

Here, we show how to deal with the contribution to  $\lambda_1'^\Lambda$  arising from diagram (a) of Fig. 3 in the OTE-momentum configuration. The Feynman integral is easily obtained from the standard one-loop expression by replacing the quark masses by  $M(q)$  and including a multiplicative factor  $Z_\psi(q)$ :

$$\begin{aligned} \lambda_1'^\Lambda(p) = & \frac{g_\Lambda^2 N}{2} \int \frac{d^d q}{(2\pi)^d} \gamma_\eta \frac{Z_\psi(q) \not{q}}{q^2 + M^2(q)} \gamma_\sigma \frac{P_{\sigma\nu}^\perp(q+p)}{(q+p)^2 + m^2} \\ & \times \frac{P_{\eta\rho}^\perp(q+p+k)}{(q+p+k)^2 + m^2} [2(q+p)_\mu \delta_{\nu\rho} - 2k_\nu \delta_{\mu\rho} + 2k_\rho \delta_{\mu\nu}] . \end{aligned} \quad (C1)$$

We first use FeynCalc to deal with the Dirac-gammas and simplify the tensorial structure. We then use FIRE [91] to reduce the integral to master integrals, taking proper care of the momentum dependence of  $M(q)$ . We find  $\lambda_1'^\Lambda = \lambda_1^\Lambda - k^2 \tau_3^\Lambda$ , with

$$\begin{aligned} \lambda_1^\Lambda(p) = & \frac{g_\Lambda^2 N}{8m^2 p^2} \int_0^\infty dq q^{d-1} Z_\psi(q) \left\{ (M^2 + p^2) (m^2 + M^2 + p^2) B(M^2, 0, -p^2) - 2m^2(d-2)A_q(M^2) \right. \\ & + \left[ 2(d-2)m^2 (m^2 - M^2 + p^2) - (M^2 + p^2)^2 \right] B(M^2, m^2, -p^2) + \left[ (2d-3)m^2 + M^2 + p^2 \right] A_g(m^2) \\ & \left. + \frac{m^2 (m^2 + 2p^2)}{2} (B(m^2, 0, -2p^2) + B(0, m^2, -2p^2) - 2(M^2 + p^2) [C(M^2, 0, m^2) + C(M^2, m^2, 0)]) \right\} \quad (C2) \end{aligned}$$

and

$$\begin{aligned} \tau_3^\Lambda(p) = & g^2 N \int_0^\infty dq q^{d-1} Z_\psi(q) \left\{ \frac{[(2d^2 - 5d + 4)m^2 + (d-1)M^2 + (7-3d)p^2] A_g(m^2)}{16(d-1)m^2 p^4} - \frac{(d-2)A_q(M^2)}{8p^4} \right. \\ & - \frac{[(d-1)M^4 + (d-2)p^4] B(0, 0, -2p^2)}{4(d-2)(d-1)m^4 p^2} + \frac{\mathcal{F}_1 [B(0, m^2, -2p^2) + B(m^2, 0, -2p^2)]}{32(d-2)(d-1)m^4 p^4} \\ & + \frac{\mathcal{F}_2 B(m^2, m^2, -2p^2)}{4(d-2)(d-1)m^4 p^4} + \frac{\mathcal{F}_3 B(M^2, 0, -p^2)}{16(d-2)m^2 p^4} + \frac{\mathcal{F}_4 B(M^2, m^2, -p^2)}{16(d-2)m^2 p^4} \\ & \left. + \frac{(M^4 + p^4) C(M^2, 0, 0) M^2}{4(d-2)m^4 p^2} + \frac{\mathcal{F}_5 C(M^2, m^2, m^2)}{4(d-2)m^4 p^4} - \frac{\mathcal{F}_6}{32(d-2)m^4 p^4} [C(M^2, 0, m^2) + C(M^2, m^2, 0)] \right\}, \quad (C3) \end{aligned}$$

where

$$\mathcal{F}_1 = (m^2 + 2p^2) [d^2 m^2 (m^2 - 4p^2) - 2dm^2 (m^2 + M^2 - 8p^2) - 2(M^4 + p^4)] + 2[m^2 (M^2 - 8p^2) - 2(M^4 + 2p^4)] \quad (C4)$$

$$\begin{aligned} \mathcal{F}_2 = & (d^2 - 3d + 2)m^6 - m^4 [(d^2 - 4d + 3)M^2 + 2(d-2)p^2] + p^2 [(1-d)M^4 - (d-2)p^4] \\ & + m^2 [(2d^2 - 9d + 10)p^4 + (1-d)M^4 + (d-1)M^2 p^2] \quad (C5) \end{aligned}$$

$$\mathcal{F}_3 = -4M^4 + 10p^2 M^2 + 6p^4 - 2m^2 p^2 + d(m^2 + M^2 - 3p^2) (M^2 + p^2) \quad (C6)$$

$$\mathcal{F}_4 = 2(d^2 - 6d + 8)m^4 - 2m^2 [(d^2 - 6d + 10)M^2 - (d^2 - 6d + 8)p^2] - (M^2 - 3p^2) [(d-4)M^2 + (d-2)p^2] \quad (C7)$$

$$\begin{aligned} \mathcal{F}_5 = & (d-2)m^8 + m^6 [(5-2d)M^2 + 2(d-2)p^2] + m^4 [(d-4)M^4 - (d-2)p^4 + 3M^2 p^2] \\ & + m^2 [(7-2d)M^2 p^4 - 2(d-2)p^6 + M^6 - 2M^4 p^2] + M^2 p^2 [M^4 + p^4] \quad (C8) \end{aligned}$$

$$\mathcal{F}_6 = (m^2 + 2p^2) [dm^2 (m^2 - 4p^2) (M^2 + p^2) - 2m^4 p^2 - 4m^2 (M^4 - 3M^2 p^2 - 2p^4) + 4M^2 (M^4 + p^4)] \quad (C9)$$

and  $M = M(q)$ . The functions  $A_q$ ,  $A_g$ ,  $B$ , and  $C$  are defined as the angular integrals over the directions of the vector  $q$

$$A_q(M^2) = \int \frac{d\Omega_d(q)}{(2\pi)^d} \frac{1}{q^2 + M^2}, \quad (C10)$$

$$A_g(m^2) = \int \frac{d\Omega_d(q)}{(2\pi)^d} \frac{1}{(q+p)^2 + m^2}, \quad (C11)$$

$$B(m_1^2, m_2^2, -p^2) = \int \frac{d\Omega_d(q)}{(2\pi)^d} \frac{1}{q^2 + m_1^2} \frac{1}{(q+p)^2 + m_2^2}, \quad (C12)$$

$$C(M^2, m_2^2, m_3^2) = \int \frac{d\Omega_d(q)}{(2\pi)^d} \frac{1}{q^2 + M^2} \frac{1}{(q+p)^2 + m_2^2} \frac{1}{(q+r)^2 + m_3^2}. \quad (C13)$$

with  $r+p+k = 0$ . We have checked that this result reproduces the one-loop expression from Ref. [67] when  $M(q)$  and  $Z_\psi(q)$  are treated as constants. The latter also reproduces results from Ref. [92] in the case of a vanishing gluon mass. In fact, because the original integral is log-

arithmically divergent, it is obvious that by adding and subtracting these perturbative expressions, we obtain one contribution that can be evaluated in dimensional regularization and another one that is explicitly finite and that can be computed directly for  $d = 4$ . In what follows

we concentrate on these latter contributions.

The next step is to perform the angular integrals analytically. For integrals involving  $A_q$ ,  $A_g$ , and  $B$ , we proceed as follows:

$$\begin{aligned} & \int_0^\infty dq q^3 w(p^2, q^2) B(m_1^2, m_2^2, -p^2) \\ &= \int_0^\infty \frac{dq q^3}{4\pi^3} \frac{w(p^2, q^2)}{q^2 + m_1^2} \int_{-1}^1 \frac{du \sqrt{1-u^2}}{q^2 + p^2 + 2qpu + m_2^2} \\ &= \int_0^\infty \frac{dq q}{16\pi^2 p^2} \frac{w(p^2, q^2)}{q^2 + m_1^2} \left( a - \sqrt{a^2 - 4p^2 q^2} \right), \quad (\text{C14}) \end{aligned}$$

with  $a = q^2 + p^2 + m_2^2$ . Integrals involving  $C$  have the generic form

$$\mathcal{H} = \int_0^\infty dq q^3 f(q^2, p^2, k^2, p.k) C(M^2, m_2^2, m_3^2), \quad (\text{C15})$$

and are computed in the following way. First, we take into account the OTE configuration, for which  $k^2 = 2p^2$  and  $p.k = -p^2$  (or, equivalently,  $p.r = 0$  and  $r^2 = p^2$ ). To perform the angular integrals, we project  $q$  in the plane defined by  $r$  and  $p$  (which are orthogonal), see Fig. 13. Then, we can write  $q^2 = q_{\parallel}^2 + q_{\perp}^2$ , with  $q_{\parallel} = q \cos \theta$  and  $q_{\perp} = q \sin \theta$ , so that

$$\int \frac{d^4 q}{(2\pi)^4} = \frac{1}{(2\pi)^4} \int d^2 q_{\perp} \int q_{\parallel} dq_{\parallel} \int_0^{2\pi} d\varphi. \quad (\text{C16})$$

Therefore,

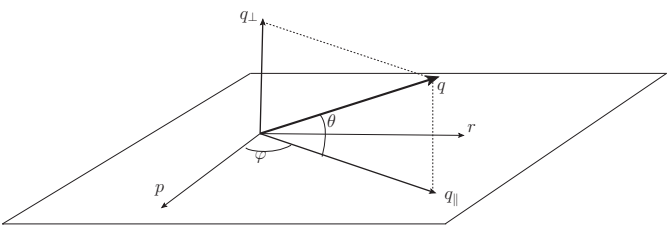


FIG. 13: OTE parametrization of the integral.

$$\begin{aligned} \mathcal{H} &= \int_0^\infty \frac{q_{\perp} dq_{\perp}}{(2\pi)^3} \int_0^\infty q_{\parallel} dq_{\parallel} \int_0^{2\pi} d\varphi \frac{f(q^2, p^2, 2p^2, -p^2)}{q^2 + M^2} \\ &\times \frac{1}{(q^2 + p^2 + 2pq_{\parallel} \cos \varphi + m_2^2)(q^2 + p^2 + 2pq_{\parallel} \sin \varphi + m_3^2)} \\ &= \int_0^\infty \frac{dq_{\perp} q_{\perp}}{2\pi} \int_0^\infty \frac{q_{\parallel} dq_{\parallel}}{2\pi} \frac{f(q^2, p^2, 2p^2, -p^2)}{q^2 + M^2} h(q^2, p^2, q^2 u) \quad (\text{C17}) \end{aligned}$$

where ( $u = \cos \theta$ )

$$h(q^2, p^2, q^2 u) = \frac{\frac{a}{\sqrt{c^2 - b^2}} + \frac{c}{\sqrt{a^2 - b^2}}}{a^2 + c^2 - b^2} \quad (\text{C18})$$

with  $b = 2pqu$  and  $c = q^2 + p^2 + m_3^2$ . Switching from the variables  $q_{\parallel}$  and  $q_{\perp}$  to  $q$  and  $\theta$ , the integral over  $\theta$  can be

evaluated as

$$\begin{aligned} \mathcal{H} &= \int_0^\infty \frac{dq q^3}{(2\pi)^2} \frac{f(q^2, p^2, 2p^2, -p^2)}{q^2 + M^2} \int_0^1 du u h(q^2, p^2, q^2 u) \\ &= \int_0^\infty \frac{dq q}{16\pi^2 p^2} \frac{f(q^2, p^2, 2p^2, -p^2)}{q^2 + M^2} \\ &\times \arctan \left( \frac{c\sqrt{c^2 - 4p^2 q^2} - a\sqrt{a^2 - 4p^2 q^2}}{ca + \sqrt{c^2 - 4p^2 q^2}\sqrt{a^2 - 4p^2 q^2}} \right). \quad (\text{C19}) \end{aligned}$$

The remaining radial momentum integral can be performed numerically using the grid that we used to determine  $M(q)$ .

#### Appendix D: Choice of kinematic configuration for the quark-gluon vertex

In this work we define the renormalized ghost-gluon coupling  $g_g$  using the Taylor scheme, that is, through the ghost-gluon vertex at vanishing ghost momentum [84]. Here, we discuss various possible definitions of the quark-gluon coupling  $g_q$  through different momentum configurations of the quark-gluon vertex. Even though the various renormalized couplings are different, they are related to the same bare value. This implies that their renormalization factors are also different. While  $Z_{g_g} \sqrt{Z_A} Z_c = 1$  for the gauge sector, in the quark sector, we have  $Z_{g_q} \sqrt{Z_A} Z_{\psi} \lambda_1'^{\Lambda} = 1$ , where  $\lambda_1'^{\Lambda}$  represents the bare quark-gluon scalar function that includes the tree-level term in the chosen kinematical configuration<sup>8</sup>. The ratio between the couplings defines the renormalized  $\lambda_1'$  as

$$\frac{g_q(\mu)}{g_g(\mu)} = \frac{Z_{\psi}(\mu)}{Z_c(\mu)} \lambda_1'^{\Lambda}(\mu) \equiv \lambda_1'(\mu). \quad (\text{D1})$$

In the UV regime we can use perturbation theory and expand this relation in  $g_g$ . In the Landau gauge, at one loop, there is no correction to the quark renormalization factor for  $\mu \gg m$  ( $Z_{\psi} = 1 + \mathcal{O}(g_g^4)$ ), while a straightforward calculation gives

$$Z_c \sim 1 + \frac{Ng_g^2}{64\pi^2} \left( \frac{6}{\epsilon} + 4 - 3 \log \left( \frac{\mu^2 e^{\gamma}}{4\pi} \right) \right) \quad (\text{D2})$$

where  $\epsilon = 4 - d$  and  $\gamma$  is the Euler constant.

Next, we determine the UV behaviour of  $\lambda_1'$  in the chosen kinematical configuration. The simplest choice is to use the vanishing-gluon-momentum configuration. In this case, the one-loop quark-gluon vertex can be computed analytically for arbitrary quark momentum  $p$ . In particular, at large momentum,

$$\lambda_1'^{\Lambda}(p) \underset{p \gg m}{\sim} 1 + \frac{3Ng_g^2}{64\pi^2} \left( \frac{2}{\epsilon} + 1 - \log \left( \frac{p^2 e^{\gamma}}{4\pi} \right) \right). \quad (\text{D3})$$

<sup>8</sup> We employ here the notation of Refs. [77, 85]. We stress that the prime here does not denote a derivative, see Eq. (37).

However, we obtain in this case

$$g_q(\mu_0) = g_g(\mu_0) \left( 1 - \frac{Ng_g^2}{64\pi^2} \right) < g_g(\mu_0). \quad (\text{D4})$$

This particular definition of the quark-gluon coupling makes it smaller than the Taylor ghost-gluon coupling in the UV, an ordering that persists in the infrared. Lattice data from [93] shows that this is not the common situation for  $\lambda'_1$  and it is then preferable to look for other configurations where the couplings are ordered in the opposite way.

It is not difficult to find such configurations. For instance, if the quark-coupling is defined using the OTE, we find for  $p \gg m$ ,

$$\lambda'_1|_{\text{OTE}}(p) \sim 1 + \frac{3Ng_g^2}{64\pi^2} \left[ \frac{2}{\epsilon} + 3 - \log \left( \frac{p^2 e^\gamma}{2\pi} \right) \right] \quad (\text{D5})$$

and, therefore,

$$g_q(\mu_0) = g_g(\mu_0) \left( 1 + \frac{g_g^2 N}{64\pi^2} (5 - 3 \log(2)) \right) > g_g(\mu_0). \quad (\text{D6})$$

In fact, we find that most configurations that contribute to the equation for the quark propagator respect the ordering  $g_q(\mu_0) > g_g(\mu_0)$ , while only a small set of configurations near the vanishing-gluon-momentum configuration give the opposite ordering  $g_q(\mu_0) < g_g(\mu_0)$ . To see this, we consider the Dyson-Schwinger equation for the quark self-energy and, for the sake of simplicity, we replace both the quark propagator and the gluon propagator by theirs tree-level-like form. Moreover, we restrict the analysis to  $\Gamma_\mu(p, q) = \gamma_\mu f(p, q)$  which is the dominant tensorial structure. The resulting contribution to the self-energy is proportional to

$$\int \frac{d^d q}{(2\pi)^d} \frac{P_{\mu\nu}^\perp(q)}{q^2 + m^2} \Gamma_\mu(p, q) \frac{q + p + M}{(q + p)^2 + M^2} \gamma_\nu. \quad (\text{D7})$$

It is easy to see that the contribution from small gluon momentum  $q \ll p, M, m$  is suppressed and that the region that dominates corresponds to  $q \sim p, M$  [50]. It follows that the vanishing-gluon-momentum scheme for the coupling is not representative and virtually any other configuration is a better option. For practical purposes we choose then the OTE configuration mentioned before.

---

[1] P. O. Bowman, U. M. Heller, D. B. Leinweber, M. B. Parappilly, A. G. Williams and J. b. Zhang, Phys. Rev. D **71**, 054507 (2005).

[2] O. Oliveira, P. J. Silva, J. I. Skullerud and A. Sternbeck, Phys. Rev. D **99**, no. 9, 094506 (2019).

[3] A. C. Aguilar and J. Papavassiliou, Phys. Rev. D **83** (2011) 014013.

[4] C. D. Roberts, M. S. Bhagwat, A. Holl and S. V. Wright, Eur. Phys. J. ST **140**, 53 (2007).

[5] H.J. Munczek, Phys. Rev. D **52**, 4736 (1995).

[6] N. Brown, and M.R. Pennington, Phys. Rev. D **38**, 2266 (1988).

[7] C. D. Roberts, and A. G. Williams, Prog. Part. Nucl. Phys. **33**, 477 (1994); C. D. Roberts, and S. Schmidt, Prog. Part. Nucl. Phys. **45**, S1 (2000); A. Bashir, et. al., Commun. Theor. Phys. **58**, 79 (2012).

[8] P. Maris, and C. D. Roberts, Phys. Rev. C **56**, 3369 (1997);

[9] P. Maris, and P. C. Tandy, Phys. Rev. C **60**, 055214 (1999);  
P. Maris and C. D. Roberts, Int. J. Mod. Phys. E **12**, 297 (2003).

[10] D. Binosi, J. Papavassiliou, Phys. Rept. **479**, 1(2009); D. Binosi, J. Papavassiliou, Phys. Rev. D **77**, 061702 (2008); D. Binosi, J. Papavassiliou, JHEP **11**, 063 (2008).

[11] R. Alkofer and L. von Smekal, Phys. Rept. **353**, 281 (2001).

[12] M.R. Pennington, and D.J. Wilson, Phys. Rev. D **84**, 119901 (2011).

[13] L. Chang, Y.X. Liu, M.S. Bhagwat, C.D. Roberts, and S.V. Wright, Phys. Rev. C **75**, 015201 (2007).

[14] K.L. Wang, S.X. Qin, Y.X. Liu, L. Chang, C.D. Roberts, and S.M. Schmidt, Phys. Rev. D **86**, 114001 (2012).

[15] L. Chang, and C. D. Roberts, Phys. Rev. Lett. **103**, 081601 (2009); Phys. Rev. C **85**, 052201(R) (2012).

[16] D. Binosi, L. Chang, J. Papavassiliou, and C.D. Roberts, Phys. Lett. B **742**, 183 (2015).

[17] D. Binosi, L. Chang, J. Papavassiliou, S.X. Qin, and C.D. Roberts, Phys. Rev. D **93**, 096010 (2016);  
Phys. Rev. D **95**, 031501 (2017).

[18] A.C. Aguilar D. Binosi, and J. Papavassiliou, Phys. Rev. D **78**, 025010 (2008).

[19] A.C. Aguilar, and J. Papavassiliou, Phys. Rev. D **83**, 014013 (2011).

[20] A.C. Aguilar D. Binosi, and J. Papavassiliou, Phys. Rev. D **86**, 014032 (2012); A. C. Aguilar, J. Papavassiliou, JHEP **12**, 012 (2006).

[21] A. Ayala, A. Bashir, D. Binosi, M. Cristoforetti, J. Rodriguez-Quintero, Phys. Rev. D **86**, 074512 (2012).

[22] J. Rodriguez-Quintero, D. Binosi, C. Mezrag, J. Papavassiliou, and C.D. Roberts, Few. Body. Syst. **59**, 121 (2018). Phenomenology”.

[23] A.L. Blum, M.Q. Huber, M. Mitter, and L. von Smekal, Phys. Rev. D **89**, 061703 (2014).

[24] G. Eichmann, R. Williams, R. Alkofer, and M. Vujinovic, Phys. Rev. D **89**, 105014 (2014).

[25] A. Athenodorou, D. Binosi, Ph. Boucaud, F. De Soto, J. Papavassiliou, J. Rodriguez-Quintero, S. Zafeiropoulos, Phys. Lett. B **761**, 444(2016); J. Rodriguez-Quintero, A. Athenodorou, D. Binosi, P. Boucaud, F. de Soto, J. Papavassiliou, S. Zafeiropoulos, EPJ Web Conf. **137**, 03018 (2017).

[26] A.C. Aguilar, J.C. Cardona, M.N. Ferreira, and J. Papavassiliou, Phys. Rev. D **96**, 014029 (2017).

[27] A. C. Aguilar, D. Binosi, J. Papavassiliou, Phys. Rev. D **95**, 034017 (2017); A. C. Aguilar, D. Binosi, C. T. Figueiredo, J. Papavassiliou, Phys. Rev. D **94**, 045002 (2016); A. C. Aguilar, D. Binosi, J. Papavassiliou, Phys. Rev. D **91**, 085014 (2015); A. C. Aguilar, D. Binosi, D. Ibanez, J. Papavassiliou, Phys. Rev. D **90**, 065027 (2014); A. C. Aguilar, D. Binosi, D. Ibanez, J. Papavassiliou, Phys. Rev. D **89**, 085008 (2014); A. C. Aguilar, D. Ibanez, J. Papavassiliou, Phys. Rev. D **87**, 114020 (2013); A. C. Aguilar, D. Binosi, J. Papavassiliou, J. Rodríguez-Quintero, Phys. Rev. D **80**, 085018 (2009).

[28] F. Akram, A. Bashir, L. X. Gutiérrez-Guerrero, B. Masud, J. Rodríguez-Quintero, C. Calcaneo-Roldan, M. E Tejeda-Yeomans, Phys. Rev. D **87**, no.1, 013011 (2013); J. Rodríguez-Quintero, JHEP **01**, 105 (2011); Ph. Boucaud, M. E. Gomez, J. P. Leroy, A. Le Yaouanc, J. Micheli, O. Pene, J. Rodriguez-Quintero, Phys. Rev. D **82**, 054007 (2010); Ph. Boucaud, M. E. Gomez, J. P. Leroy, A. Le Yaouanc, J. Micheli, O. Pene, J. Rodriguez-Quintero, Phys. Rev. D **80**, 094501 (2009); Ph. Boucaud, J. P. Leroy, A. Le Yaouanc, J. Micheli, O. Pene, J. Rodriguez-Quintero, JHEP **06**, 099 (2008); Ph. Boucaud, Th. Bruntjen, J. P. Leroy, A. Le Yaouanc, A. Y. Lohkov, J. Micheli, O. Pene, J. Rodriguez-Quintero, JHEP **06**, 001 (2006); Ph. Boucaud, J. P. Leroy, A. Le Yaouanc, J. Micheli, O. Pene, J. Rodriguez-Quintero, JHEP **06**, 012 (2008).

[29] D. Binosi, D. Ibanez, J. Papavassiliou, JHEP **09**, 059 (2014).

[30] S. X. Qin, L. Chang, H. Chen, Y. X. Liu, and C. D. Roberts, Phys. Rev. Lett. **106**, 172301 (2011).

[31] S.X. Qin, L. Chang, Y. X. Liu, and C. D. Roberts, Phys. Rev. D **84**, 014017 (2011); K.L. Wang, Y. X. Liu, L. Chang, C. D. Roberts, and S. M. Schmidt, Phys. Rev. D **87**, 074038 (2013); X.Y. Xin, S.X. Sin, and Y. X. Liu, Phys. Rev. D **90**, 076006 (2014); F. Gao, J. Chen, Y. X. Liu, S. X. Qin, C. D. Roberts, and S. M. Schmidt, Phys. Rev. D **93**, 094019 (2016); Phys. Rev. D **94**, 094030 (2016); approach” Phys. Rev. D **97**, 056011 (2018); Z. Bai, H. Chen, and Y. X. Liu, Phys. Rev. D **97**, 023018 (2018).

[32] F. Gao, and Y. X. Liu, Phys. Rev. D **94**, 076009 (2016).

[33] R. Williams, C.S. Fischer, M.R. Pennington, Phys. Lett. B **645**, 167 (2007); C. S. Fischer, D. Nickel, and R. Williams, Phys. Lett. B **718**, 1036 (2013).

[34] C. S. Fischer, J. Luecker, and J. A. Mueller, Phys. Lett. B **702**, 438 (2011); C. S. Fischer, and J. Luecker, Phys. Lett. B **718**, 1036 (2013); G. Eichmann, C. S. Fischer, and C. A. Welzbacher, Phys. Rev. D **93**, 034013 (2016).

[35] C. S. Fischer, L. Fister, J. Luecker, and J. M. Pawlowski, Phys. Lett. B **732**, 273 (2014); C. S. Fischer, J. Luecker, and C. A. Welzbacher, Phys. Rev. D **90**, 034022 (2014).

[36] C. S. Fischer, Prog. Part. Nucl. Phys. **105**, 1 (2019).

[37] C.D. Roberts, Prog. Part. Nucl. Phys. **61**, 50 (2008); I.C. Cloet, C.D. Roberts, Prog. Part. Nucl. Phys. **77**, 1 (2014); T. Horn, and C.D. Roberts, J. Phys. G **43**, 073001 (2016); C.D. Roberts, Few-Body Syst. **59**, 72 (2018). Q.W. Wang, S.X. Qin, C. D. Roberts, and S.M. Schmidt, Phys. Rev. D **98**, 054019 (2018).

[38] P. Maris, and P.C. Tandy, Phys. Rev. C **62**, 055204 (2000); R.J. Holt, and C. D. Roberts, Rev. Mod. Phys. **82**, 2991 (2010); L. Chang, I.C. Cloet, J.J. Cobos-Martinez, C.D. Roberts, S.M. Schmidt, and P.C. Tandy, Phys. Rev. Lett. **110**, 132001 (2013); Light Front ”. L. Chang, I.C. Cloet, C.D. Roberts, S.M. Schmidt, P.C. Tandy, Phys. Rev. Lett. **111**, 141802 (2013).

[39] G. Eichmann, R. Alkofer, I.C. Cloet, A. Krassnigg, and C.D. Roberts, Phys. Rev. C **77**, 042202 (2008); A. Krassnigg, Phys. Rev. D **80**, 114010 (2009); G. Eichmann, R. Alkofer, A. Krassnigg, and D. Nicmorus, Phys. Rev. Lett. **104**, 201601 (2010); G. Eichmann, Phys. Rev. D **84**, 014014 (2011); W. Heupel, G. Eichmann, and C.S. Fischer, Phys. Lett. B **718**, 545 (2012); G. Eichmann, C.S. Fischer, and W. Heupel, Phys. Lett. B **753**, 282 (2016); G. Eichmann, H. Sanchis-Alepuz, R. Williams, R. Alkofer, and C.S. Fischer, Prog. Part. Nucl. Phys. **91**, 1 (2016).

[40] C. Tang, F. Gao and Y. X. Liu, Phys. Rev. D **100**, no. 5, 056001 (2019).

[41] J. M. Pawłowski, Annals Phys. **322**, 2831 (2007).

[42] H. Gies, Lect. Notes Phys. **852**, 287 (2012) [hep-ph/0611146].

[43] J. Braun, L. Fister, J. M. Pawłowski and F. Rennecke, Phys. Rev. D **94**, no. 3, 034016 (2016).

[44] M. Mitter, J. M. Pawłowski and N. Strodthoff, Phys. Rev. D **91**, 054035 (2015).

[45] A. K. Cyrol, M. Mitter, J. M. Pawłowski and N. Strodthoff, Phys. Rev. D **97**, no. 5, 054006 (2018).

[46] R. Alkofer, A. Maas, W. A. Mian, M. Mitter, J. París-López, J. M. Pawłowski and N. Wink, Phys. Rev. D **99**, no. 5, 054029 (2019).

[47] C. Feuchter and H. Reinhardt, Phys. Rev. D **70**, 105021 (2004).

[48] H. Reinhardt and C. Feuchter, Phys. Rev. D **71**, 105002 (2005).

[49] C. S. Fischer, Prog. Part. Nucl. Phys. **105** (2019) 1.

[50] M. Peláez, U. Reinoso, J. Serreau, M. Tissier and N. Wschebor, Phys. Rev. D **96**, no. 11, 114011 (2017).

[51] A. Cucchieri, A. Maas and T. Mendes, Phys. Rev. D **77**, 094510 (2008).

[52] G. Curci and R. Ferrari, Nuovo Cim. A **32**, 151 (1976).

[53] M. Tissier and N. Wschebor, Phys. Rev. D **82** (2010) 101701.

[54] M. Tissier and N. Wschebor, Phys. Rev. D **84** (2011) 045018.

[55] V. N. Gribov, Nucl. Phys. B **139** (1978) 1.

[56] J. Serreau and M. Tissier, Phys. Lett. B **712** (2012) 97.

[57] C. Nouis, U. Reinoso, J. Serreau, R. C. Terin and M. Tissier, [arXiv:2004.12413 [hep-th]].

[58] M. Tissier, Phys. Lett. B **784**, 146 (2018).

[59] M. Peláez, M. Tissier and N. Wschebor, Phys. Rev. D **88** (2013) 125003.

[60] J. A. Gracey, M. Peláez, U. Reinoso and M. Tissier, Phys. Rev. D **100**, no. 3, 034023 (2019).

[61] N. Barrios, M. Peláez, U. Reinoso and N. Wschebor, arXiv:2009.00875 [hep-th].

[62] U. Reinoso, J. Serreau, M. Tissier and N. Wschebor, Phys. Rev. D **89**, no. 10, 105016 (2014).

[63] U. Reinoso, J. Serreau, M. Tissier and N. Wschebor, Phys. Lett. B **742** (2015) 61.

[64] U. Reinoso, J. Serreau, M. Tissier and N. Wschebor, Phys. Rev. D **91** (2015) 4, 045035.

[65] U. Reinoso, J. Serreau, M. Tissier and N. Wschebor, Phys. Rev. D **93**, no. 10, 105002 (2016).

[66] M. Peláez, M. Tissier and N. Wschebor, Phys. Rev. D **90** (2014) 6, 065031.

[67] M. Peláez, M. Tissier and N. Wschebor, Phys. Rev. D **92**, no. 4, 045012 (2015).

- [68] U. Reinosa, J. Serreau and M. Tissier, Phys. Rev. D **92**, 025021 (2015).
- [69] J. Maelger, U. Reinosa and J. Serreau, Phys. Rev. D **97**, no. 7, 074027 (2018).
- [70] J. Maelger, U. Reinosa and J. Serreau, Phys. Rev. D **98**, no. 9, 094020 (2018).
- [71] K. I. Kondo, M. Watanabe, Y. Hayashi, R. Matsudo and Y. Suda, arXiv:1902.08894 [hep-th].
- [72] F. Siringo, arXiv:1509.05891 [hep-ph].
- [73] F. Siringo, Phys. Rev. D **94**, no. 11, 114036 (2016).
- [74] F. Siringo, Phys. Rev. D **100**, no. 7, 074014 (2019).
- [75] Y. Song, G. Baym, T. Hatsuda and T. Kojo, Phys. Rev. D **100**, no. 3, 034018 (2019).
- [76] D. Suenaga and T. Kojo, Phys. Rev. D **100**, no. 7, 076017 (2019),
- [77] J. I. Skullerud, P. O. Bowman, A. Kizilersu, D. B. Leinweber and A. G. Williams, JHEP **0304**, 047 (2003).
- [78] V. A. Miransky, Nuovo Cim. A **90**, 149 (1985).
- [79] V. A. Miransky, Phys. Lett. **165B** (1985) 401.
- [80] J. A. Gracey, Phys. Lett. B **552**, 101 (2003).
- [81] Doria, R.M., Braz.J.Phys.,20, (1990) 316.
- [82] D. Dудal, H. Verschelde and S. P. Sorella, Phys. Lett. B **555**, 126 (2003).
- [83] N. Wschebor, Int. J. Mod. Phys. A **23**, 2961 (2008).
- [84] J. C. Taylor, Nucl. Phys. B **33** (1971) 436.
- [85] J. Skullerud and A. Kizilersu, JHEP **0209**, 013 (2002).
- [86] A. Sternbeck, K. Maltman, M. Muller-Preussker and L. von Smekal, PoS **LATTICE2012**, 243 (2012) doi:10.22323/1.164.0243 [arXiv:1212.2039 [hep-lat]].
- [87] U. Reinosa, J. Serreau, M. Tissier and N. Wschebor, Phys. Rev. D **96**, no.1, 014005 (2017) doi:10.1103/PhysRevD.96.014005 [arXiv:1703.04041 [hep-th]].
- [88] J. Maelger, U. Reinosa and J. Serreau, arXiv:1903.04184 [hep-th].
- [89] U. Reinosa and Zs. Szép, Phys. Rev. D **85**, 045034 (2012).
- [90] U. Reinosa and J. Serreau, JHEP **07**, 028 (2006).
- [91] A. V. Smirnov, JHEP **0810** (2008) 107
- [92] A. I. Davydychev, P. Osland and L. Saks, Phys. Rev. D **63**, 014022 (2001).
- [93] A. Sternbeck, L. von Smekal, D. B. Leinweber and A. G. Williams, PoS LAT **2007**, 340 (2007).